Remote Sensing of Environment 209 (2018) 90–106

Contents lists available at ScienceDirect

Remote Sensing of Environment

journal homepage: www.elsevier.com/locate/rse

Large-area mapping of Canadian boreal forest cover, height, biomass and other structural attributes using Landsat composites and lidar plots

Giona Matasci[a,*], Txomin Hermosilla[a], Michael A. Wulder[b], Joanne C. White[b], Nicholas C. Coops[a], Geordie W. Hobart[b], Harold S.J. Zald[c]

[a] Integrated Remote Sensing Studio, Department of Forest Resources Management, University of British Columbia, 2424 Main Mall, Vancouver, BC, V6T 1Z4, Canada
[b] Canadian Forest Service (Pacific Forestry Centre), Natural Resources Canada, 506 West Burnside Road, Victoria, BC, V8Z 1M5, Canada
[c] Department of Forestry and Wildland Resources, Humboldt State University, 1 Harpst St., Arcata, CA 95521, USA

ARTICLE INFO

Keywords:
Lidar
Landsat
Forest structure
Monitoring
Imputation
Random Forest

ABSTRACT

Passive optical remotely sensed images such as those from the Landsat satellites enable the development of spatially comprehensive, well-calibrated reflectance measures that support large-area mapping. In recent years, as an alternative to field plot data, the use of Light Detection and Ranging (lidar) acquisitions for calibration and validation purposes in combination with such satellite reflectance data to model a range of forest structural response variables has become well established. In this research, we use a predictive modeling approach to map forest structural attributes over the ~552 million ha boreal forest of Canada. For model calibration and independent validation we utilize airborne lidar-derived measurements of forest vertical structure (known as lidar plots) obtained in 2010 via a > 25,000 km transect-based national survey. Models were developed linking the lidar plot structural variables to wall-to-wall 30-m spatial resolution surface reflectance composites derived from Landsat Thematic Mapper and Enhanced Thematic Mapper Plus imagery. Spectral indices extracted from the composites, disturbance information (years since disturbance and type), as well as geographic position and topographic variables (i.e., elevation, slope, radiation, etc.) were considered as predictor variables. A nearest neighbor imputation approach based on the Random Forest framework was used to predict a total of 10 forest structural attributes. The model was developed and validated on > 80,000 lidar plots, with R^2 values ranging from 0.49 to 0.61 for key response variables such as canopy cover, stand height, basal area, stem volume, and aboveground biomass. Additionally, a predictor variable importance analysis confirmed that spectral indices, elevation, and geographic coordinates were key sources of information, ultimately offering an improved understanding of the driving variables for large-area forest structure modeling. This study demonstrates the integration of airborne lidar and Landsat-derived reflectance products to generate detailed and spatially extensive maps of forest structure. The methods are portable to map other attributes of interest (based upon calibration data) through access to Landsat or other appropriate optical remotely-sensed data sources, thereby offering unique opportunities for science, monitoring, and reporting programs.

1. Introduction

In Canada, forest ecosystems are a mosaic of trees, wetlands, and lakes, occupying an area of ~650 million ha (Wulder et al., 2008b), with a treed area of 347 million ha (Natural Resources Canada, 2016). The boreal forest, an important source of both renewable and non-renewable resources, occupies an area of 552 million ha (with 270 million ha of trees) and forms an east-west band across the country, representing a range of climatic, physiographic, and vegetation conditions (Brandt, 2009). To effectively implement sustainable management and development practices aiming at accommodating both conservation (e.g., preservation of wildlife habitats) and human use needs (e.g., building materials, fuels), boreal forests require comprehensive, timely, and accurate inventory and monitoring efforts. To this end, data collection campaigns are necessary to characterize and map forest structure, determining attributes such as canopy cover, height, biomass, stem volume as well as age, species, land-cover, and disturbance history (White et al., 2014).

The availability of accurate national forest structural information, often collected following sample-based inventories (Tomppo et al., 2010), is the foundation for satisfying a variety of science and policy information needs as well as for meeting national and international

* Corresponding author.
E-mail address: giona.matasci@gmail.com (G. Matasci).

https://doi.org/10.1016/j.rse.2017.12.020
Received 15 June 2017; Received in revised form 5 December 2017; Accepted 15 December 2017

reporting obligations (Canadian Council of Forest Ministers, 1995). However, there are important limitations of field plot-based measurements such as their cost, lack of spatial coverage, and long updating cycles. To cope with these field data collection issues, practitioners often relied upon photo plots, an expert-based interpretation of aerial imagery. For example, the Canadian National Forest Inventory (NFI) is based upon a 1% national sample as represented by 2 × 2 km photo plots established largely on a 20 × 20 km grid, supported by a subset of ground plots, collected on a panel-basis over a 10 year update cycle (Gillis et al., 2005).

More recently, Light Detection And Ranging (lidar) remote sensing technology (Baltsavias, 1999) has gained popularity as a means to obtain detailed 3-dimensional measurements of the structure of the canopy to represent forest conditions at a given place and time (Wulder et al., 2008a). As reviewed in Nelson (2013), this potential of using airborne laser-based acquisitions to study forested ecosystems was identified in the 1970s. More specifically, transects of airborne lidar data have been found to mitigate the costs of ground plot installation and offer spatially extensive and representative sampling of calibration and validation data to support the modeling of forest attributes (Wulder et al., 2012b). Wulder et al. (2012a) outline the concept of lidar plots, whereby samples of lidar are gathered (on a transect basis) to provide regional representation and spatially referenced data suitable for the development of such models.

At the same time, multispectral imagery from satellites platforms has been demonstrated as a source of data to provide spatially comprehensive characterizations of forest attributes over large areas with a level of spatial detail of relevance to the needs of forest inventory and sustainable forest management (Brosofske et al., 2014; Cohen et al., 2001; Woodcock et al., 1994). In particular, sensors of the Landsat mission such as Thematic Mapper (TM) and Enhanced Thematic Mapper Plus (ETM+) acquire reflectance products with suitable spectral and spatial resolutions that can be used as support to map vegetation conditions and dynamics (Cohen and Goward, 2004). A known limitation of medium resolution optical satellite imagery is radiometric saturation of the recorded signal when estimating vertically distributed attributes such as biomass or canopy height (Duncanson et al., 2010; Lu, 2006, 2005). When utilizing this type of data to characterize large areas, information on vertically distributed attributes can be obtained by leveraging time-series of images providing insights on forest development and succession through a reconstructed disturbance history (Pflugmacher et al., 2012). In forest ecosystems the temporal series of spectral information and related trends offers unique life-stage and succession insights to aid in the modeling of structural attributes such as stand height or biomass (Deo et al., 2017; Lu, 2006; Pflugmacher et al., 2012; Powell et al., 2010; Zald et al., 2014). The opening of the Landsat archive in 2008 (Woodcock et al., 2008) facilitated the implementation of studies utilizing the complete spatial and temporal depth of the Landsat archive (Hansen and Loveland, 2012; Wulder et al., 2008b). Additionally, there has been extensive development in routines to create composites free of atmospheric effects (Potapov et al., 2011; Roy et al., 2010; White et al., 2014). These composites can be used to detect and label change (Hermosilla et al., 2015a) as well as to uncover and quantify trends (Ju and Masek, 2016).

In recent years, there has been wide interest in developing methods relying on optical imagery to extrapolate forest structural data beyond lidar or field data coverage to represent an entire area of interest. Such approaches generally rely on statistical predictive modeling to relate localized measurements of forest conditions (e.g., lidar) and image-derived information covering broader areas (Wulder et al., 2012b). The forest/vegetation attributes of interest (canopy cover, tree height, diameter at breast height, basal area, biomass, stem volume, etc.) represent the response variables to be modeled, whereas features extracted from multispectral satellite images or other geospatial datasets such as Digital Elevation Models (DEM) or climatic layers constitute the predictor variables, or predictors. To implement these image-based spatial predictions, common methods include linear regression or Random Forest (RF) (Breiman, 2001). RF offers robust, accurate and scalable solutions to both regression and classification problems, allowing at the same time the user to gain insights on the model by means of implicitly produced variable importance measures. Application examples of RF can be found in both the remote sensing (Belgiu and Drăgu, 2016; Gislason et al., 2006) and forestry communities (Gleason and Im, 2012; Latifi et al., 2010). In forestry, another increasingly common approach is nearest neighbor (NN) imputation (Eskelson et al., 2009; Ohmann and Gregory, 2002). In contrast to regression approaches that can distort marginal distributions and covariation between Y-variables, imputation fills in missing data by substituting values from donor observations, with the underlying assumption that two locations with similar values of X-variables should be similar with respect to Y-variables. A major strength of imputation approaches is these donor-based methods are multivariate, non-parametric, and distribution-free (Eskelson et al., 2009).

Table 1 summarizes the key characteristics (type of input data, methods employed, forest attributes modeled, study area) of recent studies which combine lidar or field data and optical imagery to map forest structural attributes, recognizing that a number of studies also exist which produced carbon estimates in a laser profiling context (e.g., Nelson et al., 2017). The majority of these previous studies has tested methodologies over small areas (e.g., Ahmed et al., 2015). At the regional scale, Landsat imagery has been used in a number of studies to interpolate or extrapolate airborne lidar-based estimates of forestry productivity. Principally in forested areas these approaches have used a variety of statistical and model-based approaches to predict a range of attributes, most often height and aboveground biomass in either the US, Canada or Europe. Statistical approaches range from conventional regressions to more advanced ensemble methods like RF or regression trees such as in Hansen et al. (2016) who extrapolated Geoscience Laser Altimeter System (GLAS) tree height data with Landsat time-series in Sub-Saharan Africa. Profiling lidar data collected by the Portable Airborne Laser System (PALS) has also been used to provide high precision height measurements to be combined with GLAS pulses and Landsat-derived land-cover strata to produce local biomass and carbon estimates (Margolis et al., 2015; Neigh et al., 2013). Zald et al. (2016) applied an imputation model to map forest attributes over 50 Landsat WRS-2 scenes (forested ecozones of Saskatchewan) using a set of Landsat spectral, change and topographical predictor variables with reported accuracies in the 0.42–0.69 R^2 range when validating against independent lidar plots. Common to most of these approaches is the recognition that these technologies can inform forest management and reporting activities as well as to offer spatially explicit inputs to carbon accounting models (White et al., 2014). The level of spatial detail ultimately dictates the application and utility of a given structural map product. Studies that have been undertaken over large areas, have necessitated the use of more coarse spatial resolution imagery reducing the applicability below the regional scale. For example, Lefsky (2010) and Simard et al. (2011) both produced global tree height maps by intersecting GLAS height estimates with forest layers obtained from Moderate Resolution Imaging Spectroradiometer (MODIS) images. Also relying on MODIS imagery, Beaudoin et al. (2014) produced Canada-wide estimates of a large number of forest attributes using NFI photo plot data for calibration and validation.

In this paper, building on the regional mapping effort by Zald et al. (2016), we present a methodological framework to combine wall-to-wall Landsat surface reflectance composites, forest change information, and descriptors of topography/location to map forest attributes (including canopy cover, height, aboveground biomass and stem volume) longitudinally across a continent. In so doing, we generate information products relating to forest structure at the unprecedented spatial resolution of 30 m for the entire 552 million ha Canadian boreal forest, representing 2010 conditions. We address, document, and communicate challenges related to data processing architecture, modeling

Table 1
Summary of select studies using plots, lidar (air- or spaceborne), and optical imagery to map forest structural attributes.

Reference	Data		Method	Attributes	Study area
	Imagery	Lidar/plots			
(Hudak et al., 2002)	Landsat	Airborne	Linear regression, kriging	Height	Site in Oregon, USA
(Chen et al., 2012)	Landsat	Airborne	Spectral unmixing, geometric-optical model	Height (mean, dominant, Lorey's)	Site in Manitoba, Canada
(Tomppo et al., 2008)	Landsat, SPOT, IRS	Ground plots	k-NN	Stem volume, tree height, age	Sweden, Finland
(Ahmed et al., 2015)	Landsat (multi-temporal)	Airborne	RF, linear regression	Height	Site in British Columbia, Canada
(Lefsky et al., 2005)	Landsat (multi-temporal)	Airborne	Linear regression, unsupervised classification	Biomass	Western Oregon, USA
(Frazier et al., 2014)	Landsat (multi-temporal)	Airborne	RF	Biomass, stem volume, basal area, Lorey's height	Site in British Columbia/Yukon Territory, Canada
(Wang et al., 2016)	Landsat (multi-temporal)	Airborne	RF, linear regression, neural networks, support vector machine	Forest cover	Youyu county, Shanxi, China
(Zald et al., 2016)	Landsat (multi-temporal)	Airborne	RF-based imputation	Biomass, height, basal area, volume, canopy cover	Saskatchewan, Canada
(Huang et al., 2017)	Landsat (multi-temporal)	Ground plots	Stepwise regression, weighted group imputation	Site index, volume increment	Tahoe National Forest, California, USA
(Hansen et al., 2016)	Landsat (multi-temporal)	Spaceborne (GLAS)	Regression trees	Height	Sub-Saharan Africa
(Lefsky, 2010)	MODIS	Spaceborne (GLAS)	Decision trees, linear regression	Height	World
(Simard et al., 2011)	MODIS	Spaceborne (GLAS)	RF	Height	World
(Beaudoin et al., 2014)	MODIS	NFI photo plots	k-NN	127 attributes mapped, focus on biomass	Canada
(Boudreau et al., 2008)	Landsat (land-cover maps)	Airborne (PALS), Spaceborne (GLAS)	Linear regression	Aboveground biomass	Québec, Canada
(Neigh et al., 2013)	MODIS, ASTER, Landsat (land-cover maps)	Airborne (PALS, ALTM), Spaceborne (GLAS)	Model-based mean and variance estimations	Aboveground carbon	Boreal forest
(Margolis et al., 2015)	Landsat (land-cover maps)	Airborne (PALS), Spaceborne (GLAS)	Linear regression	Aboveground biomass	Boreal forest of North America

approach, and related implementation issues, as well as choice and availability of predictor and response variables. Our objectives are fourfold: we aim to (1) demonstrate opportunities and challenges when extending large-area mapping studies to the national scale with the synergistic use of Landsat pixel composites and lidar plots, (2) generate accurate 30-m spatial resolution maps of forest attributes spanning the Canadian boreal forest, (3) provide insights on the key drivers of the modeling process over such large spatial extents by investigating the relevance of the predictor variables, and (4) yield reliable estimates of the average aboveground biomass and gross stem volume available in each ecozone.

2. Study area

We focus our prediction and mapping on the Canadian boreal zone, as defined by Brandt (2009), an area of 552 million ha. Ecozones are used to summarize model predictions at meaningful ecological and geographical scales (Ecological Stratification Working Group, 1996) and enable focus on those which are in the boreal zone: Atlantic Maritime, Boreal Cordillera, Boreal Plains, Boreal Shield East, Boreal Shield West, Hudson Plains, Taiga Cordillera, Taiga Plains, Taiga Shield East, Taiga Shield West. Fig. 1 shows the study area and the extent of the lidar transects with respect to ecozones and boreal forest.

These forested ecozones of the Canadian boreal feature a patchwork of land-cover categories dominated by trees, wetlands, lakes, and shrubs. The treed lands are comprised of both deciduous and coniferous tree species, dominated by white spruce (*Picea glauca*), black spruce (*Picea mariana*), balsam fir (*Abies balsamea*), jack pine (*Pinus banksiana*), trembling aspen (*Populus tremuloides*), and balsam poplar (*Populus balsamifera*). The main source of disturbance across the region is wildfire (Kurz and Apps, 1999), with large areas of a variable extent that burn on an annual basis in the unmanaged northern forests. The following ecozones are especially impacted by this type of disturbance: Boreal Cordillera, Boreal Plains, Boreal Shield East and West, Hudson Plains, Taiga Cordillera, Taiga Plains, Taiga Shield East and West. The southern reaches of the boreal forest (Atlantic Maritime, Boreal Plains, Boreal Shield East and West, as well as Taiga Plains ecozones) are subject to industrial and timber harvesting activities (White et al., 2017), as well as fire suppression activities that serve to reduce the regional impact of wildfires (Wulder et al., 2004). Another type of disturbance affecting the boreal forest is related to insect-induced stand mortality (Brandt et al., 2013; Kurz and Apps, 1999).

3. Data

3.1. Lidar data

During the summer of 2010, a national lidar data acquisition campaign took place, comprising 34 survey transects (Fig. 1) of > 25,000 km in total length. A series of constraints (suitability of airports runways, fuel availability, maintenance facilities) dictated the choice of the flight lines. Discrete return lidar data was acquired by fixed-wing aircraft equipped with an Optech ALTM 3100 laser scanner. The survey specifications were the following: flying height of 1200 m above ground level, 70 kHz pulse rate, scan angle of ± 15 from nadir resulting in a nominal pulse density of 2.8 returns per m^2 with an expected nominal footprint size of ~30 cm, given a laser beam divergence of 0.3 mRad (see Wulder et al., 2012a; Wulder et al., 2012b for details). The effective swath width of the transect (~800 m) is the product of flight parameters and instrument settings (Bater et al., 2011). Similar to best practice guidelines in lidar-based forest inventory (White et al., 2013), a 25 × 25 m grid was used to tessellate the lidar point cloud data into grid-based metrics. From a total of > 32 million lidar plots, > 17 million were treed based on intersection with the land-cover data from the Earth Observation for Sustainable Development of forests (EOSD) map (see Wulder et al., 2008b, available online at: http://tree.pfc.

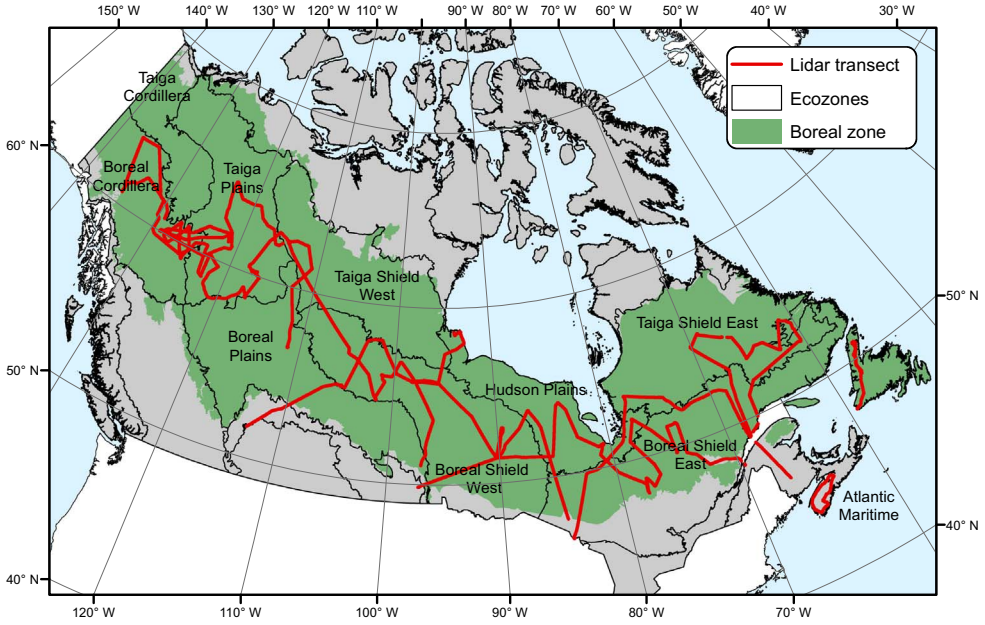

Fig. 1. Study area encompassing the boreal forest of Canada with ecozone boundaries and the path of the ~25,000 km of airborne lidar transects.

forestry.ca/). Using the publicly available software FUSION (McGaughey, 2013), a number of variables describing the lidar returns in each grid cell were calculated from classified lidar point cloud files (ground vs. non-ground). These attributes describe the vegetation structure in terms of height, cover, and vertical distribution of vegetation.

For this study, we selected six point cloud distribution metrics, or lidar metrics, as response variables for our statistical modeling approach via imputation (first 6 rows of Table 2). To compute them, initially, the lidar first returns found within the same cell are identified. For the first four metrics (elev_mean, elev_sd, elev_cv, elev_p95), the corresponding descriptive statistics (mean, standard deviation, coefficient of variation, 95th percentile) are calculated based on the recorded height of these first returns. The metrics cover_2m and cover_mean are derived by dividing the number of first returns above 2 m (or above the mean height of the first returns) by the total number of first returns within a given cell. Additionally, four derived forest structure variables and total aboveground biomass estimates, hereafter referred to as forest attributes, were considered in the mapping process, but only as auxiliary variables to be attached to each new sample whose values are being imputed (last 4 rows of Table 2). These forest attributes were derived from lidar metrics by applying regression models developed on 201 field plots located in Quebec, Ontario, and the Northwest Territories (see Wulder et al., 2012a for details). The plot positions were measured following recommended practices (i.e., mapping-grade GPS receivers, differential correction (White et al., 2013)). The potential residual mismatch between these plots and the lidar acquisitions has been deemed negligible in view of the spatial auto-correlation displayed by both the forest attributes and the lidar metrics (Zald et al., 2014).

Table 2
Response variables directly measured or derived from the lidar acquisitions. Basal area and gross stem volume were calculated for trees at 1.3 m above ground level. Total aboveground biomass includes estimates of foliage, branches, crown, bark, wood, and stem biomass.

Source	Variable name	Description	Unit
Directly measured from lidar	elev_mean	Mean of first returns height	m
	elev_sd	Standard deviation of first returns height	m
	elev_cv	Coefficient of variation of first returns height	–
	elev_p95	95th percentile of first returns height	m
	cover_2m	Percentage of first returns above 2 m	%
	cover_mean	Percentage of first returns above mean height of first returns	%
Derived from lidar	loreys_height	Lorey's tree height	m
	basal_area	Basal area	m^2/ha
	stem_volume	Gross stem volume	m^3/ha
	ag_biomass	Total aboveground biomass	t/ha

3.2. Landsat data

The source for the spectral and change-related predictor variables consisted of a suite of Landsat pixel-based composites. Seamless surface reflectance composites covering the forested ecosystems of Canada were available for each year of the 1984–2012 period, as described in detail in Hermosilla et al. (2015b). Following the Composite-to-Change (C2C) approach presented in Hermosilla et al. (2015a), layers with the year and type of disturbance for each pixel were also available. The C2C disturbance products are open data and can be obtained at: https://opendata.nfis.org/mapserver/nfis-change_eng.html. The main steps for the generation of these products are summarized in Hermosilla et al. (2016).

To generate the Landsat pixel composites addressing atmospheric effects, ensuring gap-free coverage, and controlling for phenology, a best-available-pixel (BAP) approach (White et al., 2014) has been implemented (Hermosilla et al., 2015b). Candidate TM/ETM+ images included those acquired ± 30 days of August 1st (Julian day 213) with < 70% cloud cover and were downloaded from the United States Geological Survey (USGS) Landsat Archive as Level-1 Terrain Corrected (L1 T) products. Surface reflectance was then calculated using LEDAPS (Masek et al., 2006). Of the 1285 scenes (path/rows) of the Landsat Worldwide Referencing System (WRS-2) that represent Canada, 73,544 images contributed to the generation of the final composite products (3568 for the 2010 composite). Utilizing a scoring system that weighted sensor type (prioritizing Landsat TM over ETM+ post-scan line corrector failure beginning in 2003), distance to clouds/cloud shadows (screened using Fmask (Zhu and Woodcock, 2012)), atmospheric opacity (from LEDAPS), and proximity to target date, at each pixel location the BAP across all candidate images was determined and used to build

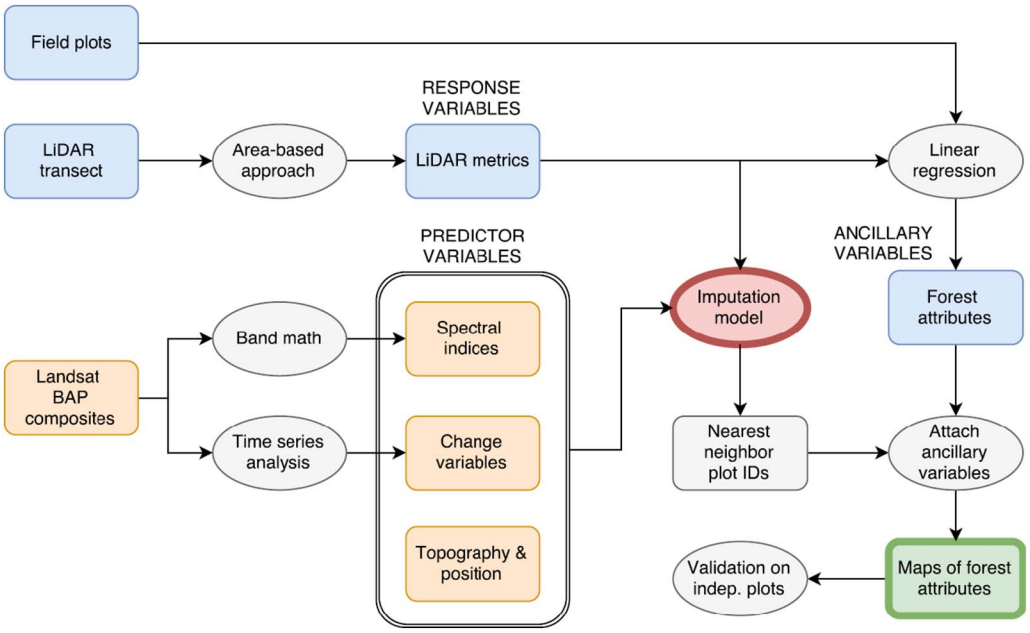

Fig. 2. Workflow adopted for the modeling and mapping of forest attributes across the Canadian boreal forest.

the final annual composite. Additional assessment of each pixel from the time series of annual imagery was undertaken using the temporal sequence of reflectance for each pixel to remove any remaining atmospheric effects (e.g., haze, smoke) and ensure complete spatial and temporal coverage of the composites (Hermosilla et al., 2015b). As such, data gaps that exist after the initial BAP compositing step (pixel screening) are addressed with the assignment of proxy values following a pixel-level time series analysis, as described in Hermosilla et al. (2015b) and Hermosilla et al. (2016).

Using the pixel level temporal series, the C2C methodology enabled the computation of several time-series trend metrics describing the magnitude, duration, and date of the detected disturbances (Hermosilla et al., 2015a). A RF classification model was trained based on a set of change events labeled by photo-interpretation from high spatial resolution imagery enabling the classification of the detected change events into a change type, including fire, harvesting, infrastructure, and non-stand replacing changes (Hermosilla et al., 2015a).

3.3. Digital elevation model

The ASTER Global Digital Elevation Map (GDEM, v. 2) was used to derive the variables describing the topography to inform models with locally relevant information on landscape position. In June 2009, a first version of the ASTER GDEM generated using stereo-pair images collected by the ASTER instrument onboard the Terra satellite was released. In 2011, an additional 260,000 stereo-pairs to increase spatial coverage and to reduce artifacts resulted in an improved version 2 of the ASTER GDEM. The current version of this DEM, derived using an updated set of algorithms, has an effective spatial resolution of 70 m (with the final product oversampled to an application-ready 30 m grid resolution), with reported improvements to horizontal (0.23 pixels) and vertical (17 m at the 95% confidence level) accuracies (Tachikawa et al., 2011). As a global product, GDEM v.2 provides both the spatial coverage and spatial resolution (30 m grain) to be well matched as a supplemental data layer for informing land-cover classification in conjunction with Landsat imagery (Franklin et al., 2003).

4. Methods

The proof of concept study by Zald et al. (2016) provides the foundation for the research presented herein, where the authors applied an imputation model over a 37 million ha area (50 WRS-2 Landsat scenes) corresponding to the forested ecozones of Saskatchewan, Canada. The model is based upon a set of spectral, change, and topographic predictor variables with reported accuracies in the 0.42–0.69 R^2 range for all considered forest attributes when validating the maps using 1085 independent lidar plots.

In Fig. 2, we graphically summarize the main methodological steps of the approach we implemented in the present study. To build the dataset with response and predictor variables values to develop the statistical model, a series of co-located measurements of the 2010 lidar/forest attributes and corresponding spectral/change/topographical features was needed. After training, the RF-based imputation model is assessed on independent validation plots and ultimately applied across the boreal forest to obtain the forest attributes maps.

4.1. Sample selection

The 25-m resolution grid of lidar survey plots (see Section 3.1), was sub-sampled to provide meaningful training and validation plots. To avoid spatial autocorrelation, a 250-m hexagon lattice was overlain on the lidar transects and the 25-m cell located in the center of each hexagon was selected as a plot (see Zald et al., 2016). Subsequently, to avoid biases stemming from high scan angles at transect edges, small plot sizes, non-vegetation outliers (e.g., towers), forest edge effects and mixed structural conditions (heterogeneous plots with multiple forest conditions), lidar plots were retained if they met the following criteria:

- located < 300 m away from the center of the lidar transect,
- associated with 95th percentile of first returns height (elev_p95) values lower than 60 m,
- in a 90 × 90 m polygon surrounding the plot, all of the plots were in a treed area, as delineated in the EOSD project,
- all of the adjacent plots (3 × 3 neighborhood) were either disturbed or undisturbed, as determined from the 1984–2012 disturbance history for Canada (Hermosilla et al., 2015a), and
- in the same 3 × 3 neighborhood, the coefficient of variation of elev_p95 was lower than 50%.

After filtering, the total number of lidar plots was 80,687, of which

Table 3
Training and validation plots count by ecozone.

Ecozone	# training samples	# validation samples
Atlantic Maritime	2894	950
Boreal Cordillera	11,552	3853
Boreal Plains	2233	754
Boreal Shield East	13,418	4453
Boreal Shield West	12,069	4035
Hudson Plains	3797	1264
Taiga Plains	7125	2372
Taiga Shield East	5499	1868
Taiga Shield West	1918	633

75% were randomly sampled to be included in the training set (60,505 samples), leaving the remaining 25% (20,182 samples) to form an independent validation set for model assessment. Table 3 breaks down by ecozone the number of samples found in the training and validation sets.

Fig. 3 shows the distribution by ecozone of the lidar metric elev_p95 across the training and validation data set. As expected, a latitudinal gradient exists, with the northerly Taiga ecozones having the shortest tree heights. Longitudinally, distribution of vegetation height across Canada's boreal forest tends to decrease from the tallest trees located in the easternmost Atlantic Maritime ecozone to shorter trees located in the more northerly, wetland dominated, Hudson Plains, to then increase again as moving westward towards the Boreal Cordillera.

4.2. Predictor variables

The initial predictor variables for the statistical analysis were Landsat-derived spectral indices and change variables, topographic variables, as well as the geographic coordinates (latitude and longitude) (Table 4). They were selected to avail upon unique spectral information (spectral channels and indices) as well as supplemental information to offer increased predictive power and statistical separability, such as landscape characteristics (from elevation data) or successional stage (from change data). Aiming to use a parsimonious and statistically informative set of predictors, we built upon the rationale, predictors, and the variable importance analysis presented in Zald et al. (2016). The Landsat composites for the year 2010 (see Section 3.2) enabled calculation of Tasseled Cap transformation brightness (TCB), greenness (TCG), and wetness (TCW) (Crist and Cicone, 1984; Kauth and Thomas, 1976). From these variables, Tasseled Cap angle (TCA) (Powell et al., 2008) and distance (TCD) (Duane et al., 2010) were calculated as follows: $TCA = \arctan(TCG/TCB)$, $TCD = (TCG^2 + TCB^2)^{1/2}$. TCA relates to the gradient of vegetation cover, whereas TCD is a function of vegetation composition and structure. Additionally, the Enhanced Vegetation Index (EVI) (Gao et al., 2000; Huete et al., 1997) and the Normalized Burn Ratio (NBR) (Key and Benson, 2005) were also extracted from the spectral bands.

The Landsat-derived forest-change metrics included the number of years since greatest change (YrsSince_GrCh), and the attributed change type (Ch_attr). YrsSince_GrCh was computed by subtracting from the mapping year the year of the breakpoint associated with the change whose magnitude is the greatest in that pixel's history (Hermosilla et al., 2015a). Since changes could be detected only starting from 1985 forward, possible values for this variable were [0, 1, …, 24, 25, 50], where 50 indicates a pixel that was never detected as changed during the Landsat time series. The latter has been set arbitrarily to a value larger than 25 to avoid confusion, recalling that for a RF model only the ranks of the samples in each predictor variable matter. Ch_attr is a categorical variable with 5 classes conveying the type of disturbance, as determined in Hermosilla et al. (2015a): no change, wildfire, harvest, non-stand replacing and infrastructure.

From the GDEM elevation data we calculated the slope (in degrees), the topographic wetness index (TWI) (Beven and Kirkby, 1979) and the topographic solar radiation index (TSRI) (Roberts and Cooper, 1989). The TWI is a model of potential surface moisture based local upslope contributing area and slope, where TWI = ln(specific catchment area/tan(slope in radians)). TSRI is a transformed measure of aspect (directional topographic exposure) obtained as $TSRI = 0.5 - \cos((\pi/180)(aspect - 30))/2$. TSRI can range between 0, indicating cold NE slopes, and 1, indicating warm SW slopes. We therefore included as predictors the elevation (Elev), the slope (Slope), the TWI and the TSRI. These topographic variables after reprojection and resampling were aligned with the predictors extracted from the Landsat pixel composites and at the same spatial resolution (30 m).

For data organization and computational considerations, each raster source dataset (surface reflectance BAP proxies, GDEM layer) was partitioned into UTM zone-related processing tiles. The approach, initially adopted to manage the Landsat datasets in Hermosilla et al. (2016), consists of dividing the country longitudinally into bands corresponding to UTM zones 7 to 22 and then further dividing each one of them into three latitudinal zones (South, North, Arctic). By sequentially looping through the 17 UTM referenced tiles that intersected the lidar transect, and by reprojecting the vector layers of the plot polygons into the same UTM zone projection, we could extract the predictor variable values in correspondence to each training and validation plot. As a spatial mismatch between the lidar plot polygons and the pixels of the raster layers (25-m vs. 30-m cell size, unaligned grids) still existed after reprojection, to assign a unique value to each plot we computed a weighted mean where the weight of each contributing pixel was equal to the proportion of its surface covered by the plot polygon. We adopted this method for all the variables except for YrsSince_GrCh and Ch_attr, where the value of the pixel under the center of the plot was recorded. As the forest attributes being mapped are spatially autocorrelated at a local scale, the geographic position of the training plots relative to the mapping grid was deemed an important factor. Thus, we added the spatial coordinates of the samples, longitude (Long) and latitude (Lat), as predictor variables.

Given the expectation that imputation could be impacted if too many highly correlated predictors are provided as input, we analyzed the correlation matrix of the predictors to select a meaningful subset to provide as input to the models. The analysis was restricted to continuous variables, therefore retaining by default the change variables (YrsSince_GrCh and Ch_attr). In the correlation matrix (Table 5), we highlighted the pairs of variables having an absolute correlation coefficient $|R| \geq 0.95$. For each of these pairs, to ensure complementarity among predictors, variables that presented the highest average $|R|$ with the remainder of the predictors were removed. This procedure resulted in the elimination of EVI and TCD, leaving 13 predictors for the analysis: TCB, TCG, TCW, TCA, NBR, YrsSince_GrCh, Ch_attr, Elev, Slope, TWI, TSRI, Long, Lat.

4.3. Imputation approach

Following Zald et al. (2016), we adopted a NN imputation methodology (k-NN with $k = 1$), an approach that aims to fill in missing observations for the response variables (Y-variables) with existing reference measurements by relating them to predictor variables (X-variables) that exist for all samples. In contrast to other methods that model each response variable separately, when $k = 1$, imputation associates to each new sample the complete set of measured response variable values of a particular training sample.

To find the optimal training sample to impute, that is, the nearest neighbor, the method utilizes a multivariate measure of distance between samples that can be provided by techniques such as canonical correlation analysis (Moeur and Stage, 1995), canonical correspondence analysis (Ohmann and Gregory, 2002), or ensemble machine learning methods such as RF (Deo et al., 2017; Henderson et al., 2014;

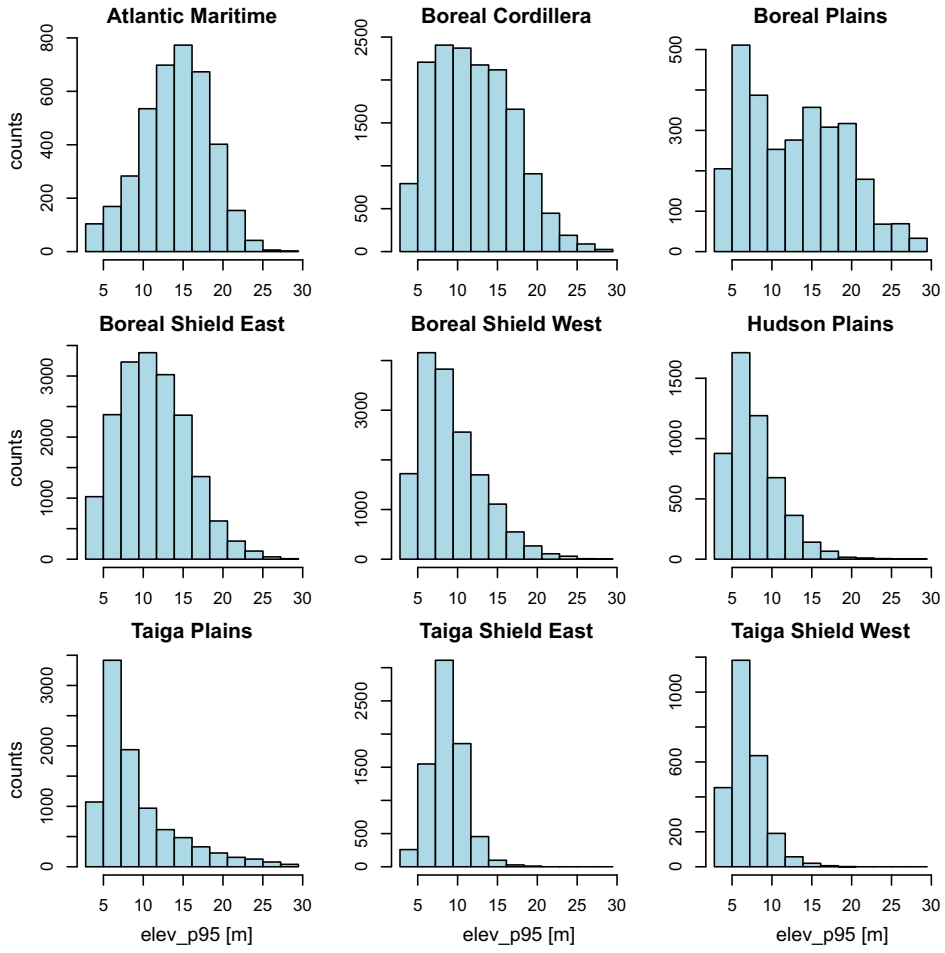

Fig. 3. Frequency distribution across the 9 sampled ecozones of the response variable elev_p95 (training and validation set).

Table 4
Predictor variables available across the mapping area.

Type	Variable name	Description
Spectral indices	TCB	Tasseled Cap brightness
	TCG	Tasseled Cap greenness
	TCW	Tasseled Cap wetness
	TCA	Tasseled Cap angle (Powell et al., 2008)
	TCD	Tasseled Cap distance (Duane et al., 2010)
	EVI	Enhanced Vegetation Index (Huete et al., 1997)
	NBR	Normalized Burn Ratio (Key and Benson, 2005)
Change variables	YrsSince_GrCh	Year in which the greatest change breakpoint occurs, subtracted from prediction year (2010) (Hermosilla et al., 2016)
	Ch_attr	Type of change attributed in Hermosilla et al. (2016)
Topography	Elev	Elevation above sea level in meters
	Slope	Slope in degrees
	TWI	Topographic wetness index (Beven and Kirkby, 1979)
	TSRI	Topographic solar radiation index (Roberts and Cooper, 1989)
Geographical	Long	Longitude in degrees
	Lat	Latitude in degrees

Hudak et al., 2008).

For the imputation approach used herein, the RF proximity matrix is used to derive a nearest neighbor distance metric (Liaw and Wiener, 2002). This distance is a non-Euclidean measure computed as one minus the proportion of trees where the new sample shares the terminal node (leaf) with a training sample (Crookston and Finley, 2008). These frequencies are computed across the trees of all the RF models that are each tuned to a single response variable. This nearest neighbor is the sample that best fits all the response variables at the same time. Once it is found, the training sample identifier is returned and its response variable scores, all together, are assigned to the new sample to be predicted. One of the main characteristics of imputation is the preservation of the covariance structure among the response variables when $k = 1$. In addition, it is important to note that the methodology will respect the range of values found in the training data, as the predicted values will be the exact same values of a plot found in the training set.

In this study, we trained the imputation model on six response variables from the lidar plots (see Table 2): elev_mean, elev_sd, elev_cv, elev_p95, cover_2m and cover_mean. Derived forest structure and biomass attributes of the corresponding training plots were then attached as auxiliary variables to the imputation predictions for each new sample. That is, these variables were not modeled by the different RFs, but rather passively transferred after training plot identifiers were predicted for each new sample.

We utilized the R package *yaImpute* (Crookston and Finley, 2008), itself based on the package *randomForest* (Liaw and Wiener, 2002). After preliminary exploratory analyses, the parameters retained were as follows: the number of variables to test at each node was selected based on the square root of the number of predictors (i.e., *mtry* = 3) and the number of trees (*ntree*) was set to 100. As we did not observe marked performance improvements by raising it, the number of trees has been kept relatively low to ensure tractable computational times in the

Table 5
Correlation matrix among predictors (with the exclusion of YrsSince_GrCh and Ch_attr) computed over the complete set of sampled plots (80,687). |R| ≥ 0.95 are in bold.

	TCB	TCG	TCW	TCA	TCD	EVI	NBR	Elev	Slope	TWI	TSRI	Long	Lat
TCB	1.00												
TCG	0.57	1.00											
TCW	− 0.62	0.04	1.00										
TCA	0.10	0.84	0.47	1.00									
TCD	**0.98**	0.70	− 0.53	0.26	1.00								
EVI	0.70	**0.97**	− 0.12	0.73	0.80	1.00							
NBR	0.01	0.68	0.70	0.90	0.15	0.57	1.00						
Elev	− 0.16	− 0.16	0.06	− 0.09	− 0.17	− 0.16	− 0.06	1.00					
Slope	− 0.06	0.07	0.10	0.12	− 0.03	0.06	0.10	0.56	1.00				
TWI	0.01	0.03	0.00	0.03	0.02	0.04	0.01	0.24	0.22	1.00			
TSRI	0.06	0.03	− 0.05	0.01	0.06	0.04	− 0.01	− 0.03	− 0.03	− 0.08	1.00		
Long	0.25	0.31	0.05	0.25	0.28	0.31	0.26	− 0.50	− 0.18	0.04	0.01	1.00	
Lat	− 0.26	− 0.49	− 0.14	− 0.46	− 0.33	− 0.46	− 0.43	0.50	0.18	− 0.01	− 0.01	− 0.88	1.00

mapping phase involving such a massive dataset. It is worth noting that, as the implementation in *yaImpute* shares the number of trees across the individual RF models, when specifying the input parameters, we had to multiply this value by the number of modeled response variables, six in our case, to truly have RF models with 100 trees.

4.4. Model assessment

The model was assessed using 20,182 validation samples by comparing imputed to observed values using a series of goodness of fit measures, including the coefficient of determination R^2, root mean squared error (RMSE) and RMSE expressed as a percentage of the observed mean (RMSE%) for each response variable. We also report the unsystematic (AC_u, a measure of random error) and systematic (AC_s, a measure of bias) agreement coefficients (Ji and Gallo, 2006) as well as the prediction bias (average of predicted minus observed values). The agreement coefficients are based on the geometric mean functional relationship (GMFR) regression line (Draper and Smith, 1998), which is a symmetric regression model that assumes both X-variables and Y-variables are subject to error (contrary to ordinary least squares regression). AC_s represents the difference between observed and predicted values that can be predicted by a simple linear model (bias from the 1:1 line, with $AC_s = 1$ if the GMFR line is perfectly aligned with the 1:1 line), whereas AC_u represents differences which appear to be random (scatter around the GMFR line, with $AC_u = 1$ if all points fall directly on it).

4.5. Variable importance in Random Forest-based imputation

To understand which predictive variables drive the model predictions we studied the variable importance scores provided by RF (Breiman, 2001). In a regression problem, these scores are determined as follows. In each of the *ntree* trees of the RF, the out-of-bag Mean Squared Error (MSE) is first stored. Then, in turn, each one of the predictors is permuted (values randomly reassigned among the set of out-of-bag samples) and the difference in MSE, usually an increase, is computed and averaged over all the trees. Finally, normalization by the standard deviation of the differences is carried out to represent the output as a percentage of increase in MSE. In the case of a RF-based imputation, this series of steps is carried out separately for each RF model (one for each one of the 6 response variables). To ensure values are expressed in a comparable scale, for each response variable, the scores of all the predictors are standardized to have a zero-mean and a unit standard deviation.

4.6. Forest attributes mapping and estimates by ecozone

The validated imputation model was ultimately applied on the raster layers of the predictor variables (spectral indices, change and topography variables, plus the extracted coordinates) across the extent of the Canadian boreal forest. Training plot IDs were predicted at each pixel location and the corresponding attribute profile was assigned. This assignment was undertaken for all pixels in treed areas, as determined from a 2010 Canada-wide land-cover map (Hermosilla et al., 2018). Based on their respective attributes maps, exhaustive estimates of gross stem volume and total aboveground biomass were derived from all the mapped pixels in each ecozone within the boreal forest. In this step, the Atlantic Maritime ecozone was not considered, as only a small area of this ecozone is included within the boreal zone.

5. Results

5.1. Model assessment

5.1.1. Global accuracy assessment in the boreal forest

Table 6 summarizes the results of the accuracy assessment

Table 6
Summary statistics for the observed and predicted lidar metrics and forest attributes with associated accuracy measureson the 20,182 validation plots.

		Observed				Predicted				Accuracy metrics					
Resp. variable	Units	Mean	Min	Max	Std. dev.	Mean	Min	Max	Std. dev.	R^2	RMSE	RMSE%	AC_u	AC_s	Bias
elev_mean	m	6.38	2.11	29.84	3.16	6.36	2.13	31.03	3.17	0.49	2.45	38.4	0.259	1	− 0.02
elev_sd	m	2.36	0.06	54.17	1.31	2.33	0.11	11.12	1.24	0.377	1.12	47.5	− 0.007	0.996	− 0.02
elev_cv	–	0.37	0.03	4.37	0.1	0.37	0.05	1.02	0.1	0.126	0.11	29.7	− 0.86	0.994	0
elev_p95	m	10.39	2.22	34.94	4.64	10.33	2.25	36.34	4.61	0.495	3.56	34.3	0.297	1	− 0.06
cover_2m	%	42.17	0.27	100	27.94	42.21	0.37	100	27.89	0.612	18.41	43.7	0.51	1	0.04
cover_mean	%	20.45	0.1	71.47	15.21	20.51	0.12	68.78	15.22	0.584	10.44	51.1	0.459	1	0.06
loreys_height	m	11.11	3.72	27.16	3.57	11.06	3.76	27.95	3.54	0.5	2.72	24.5	0.309	1	− 0.05
basal_area	m^2/ha	13.59	0.87	79.75	9.51	13.53	1.07	74.3	9.51	0.544	6.89	50.7	0.366	1	− 0.06
stem_volume	m^3/ha	90.85	1.67	1031	92.27	90.31	2.24	919.7	92.57	0.491	71.51	78.7	0.241	1	− 0.54
ag_biomass	t/ha	52.89	1.92	448.6	45.72	52.62	2.42	407.4	45.79	0.515	34.37	65.0	0.302	1	− 0.26

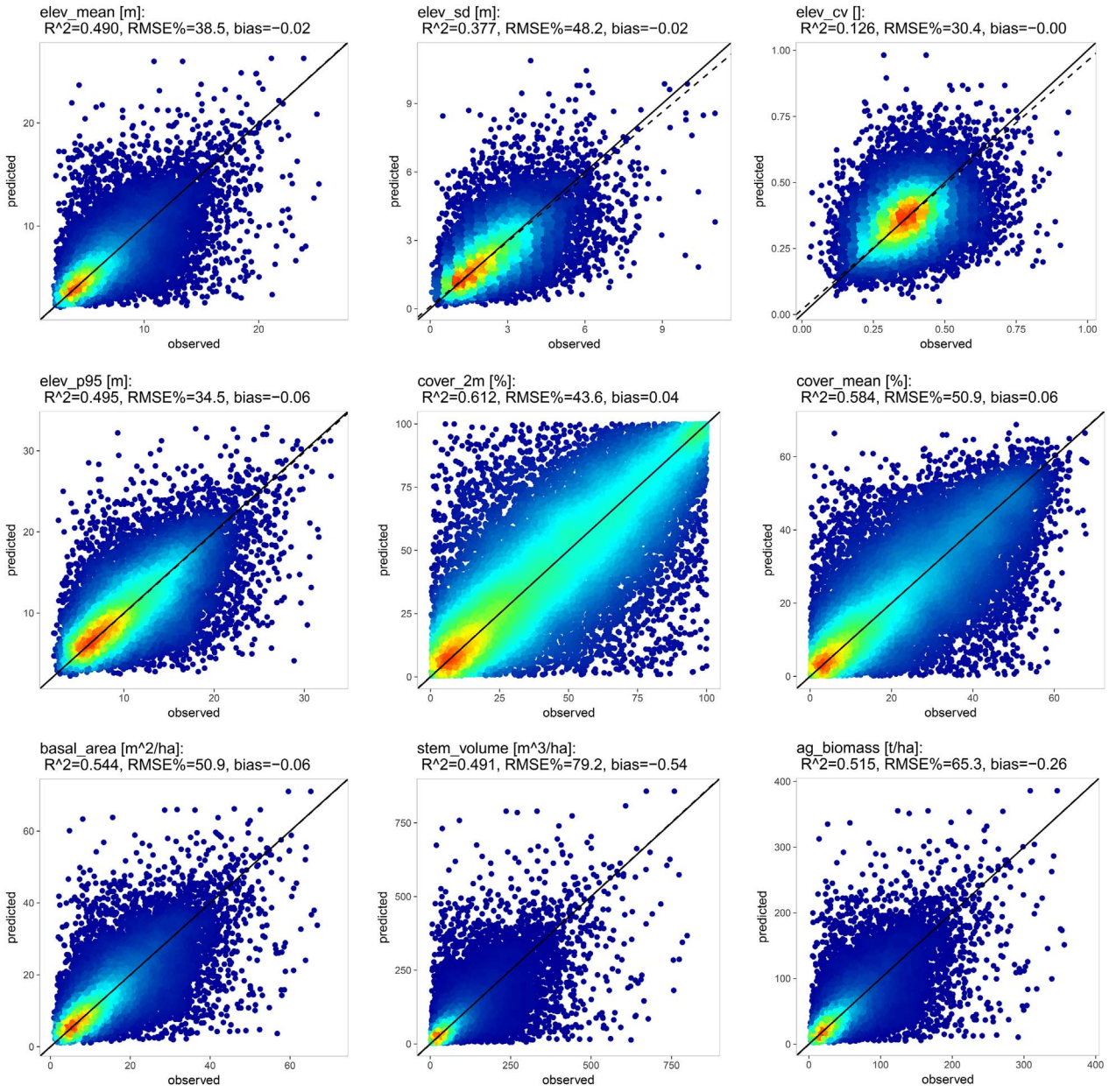

Fig. 4. Observed versus predicted values for selected response variables (omission of loreys_height) on the 20,182 validation plots. 1:1 line in solid black, GMFR line between observed and predicted values in dashed black. Point density is indicated with a blue (low-density regions) to red (high-density regions) color gradient. (For interpretation of the references to color in this figure legend, the reader is referred to the web version of this article.)

conducted on the 20,182 validation plots distributed across the entire lidar transect. The main descriptive statistics (mean, range and standard deviation) of the observed and predicted values match closely, as was expected due to the nature of the imputation approach (i.e., assign as a set the values of an existing plot). The R^2 metric is in the 0.49–0.61 range for all response variables except for those conveying the variability of lidar first returns height (elev_cv: $R^2 = 0.126$, elev_sd: $R^2 = 0.377$). RMSE values in the prediction of the height of the trees in the plot are of approximately 2.5 m for the mean height (elev_mean), 3.6 m for the height of the tallest trees (elev_p95) and 2.7 m for the mean height weighted by basal area (loreys_height). Response variables related to canopy cover present an RMSE of 18.4% (cover_2m) and 10.4% (cover_mean). Gross stem volume and aboveground biomass values registered RMSE values of 71.5 m^3/ha and 34.4 t/ha, respectively. The agreement coefficients AC_u and AC_s indicate that, although the model presents little bias (AC_s values very close or equal to 1), there is still significant amount of variability in the estimates that it is not able to explained, especially for attributes relating to the variance of first returns height (AC_u scores that are negative).

In Fig. 4, we report the corresponding scatterplots of observed versus predicted values for the response variables. The absence of bias is visible as there is no underestimation of high values or overestimation of low values in all the plots (1:1 line and GMFR line are almost indiscernible). The scatter around the 1:1 line is within reasonable limits for the vast majority of the samples. Outliers with large errors (both over- and under-estimates) are present, but are associated with a minority of the dataset.

5.1.2. Accuracy assessment in each ecozone

Fig. 5 depicts the mapping accuracy on validation plots within each boreal ecozone covered by the transect for three response variables representing key forest structural attributes: elev_p95, cover_2m, ag_biomass. For the majority of ecozones and attributes, R^2 exceeds 0.4, with the greatest accuracies, on average, being observed in the Taiga

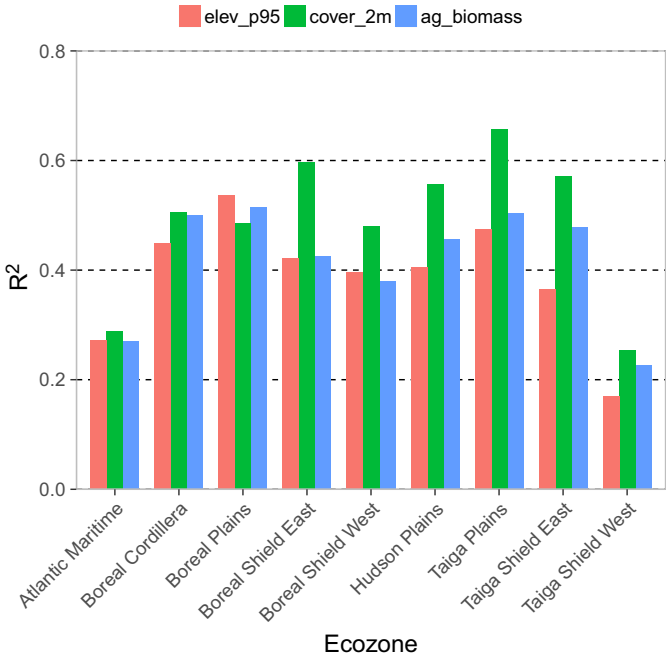

Fig. 5. R^2 values for the response variables elev_p95, cover_2m, ag_biomass on validation plots split by ecozone.

Plains, Boreal Plains and Boreal Cordillera ecozones. The figure highlights poorer predictions for the Atlantic Maritime and Taiga Shield West ecozones, both of which have $R^2 < 0.3$ for all these three variables. Fig. 6 shows the distribution of the residuals by ecozone for the elev_p95 variable and reveals how these are highly symmetrical with respect to the residual value of zero, indicating no systematic bias in the predictions. The spread of the bins around the zero value is relatively small for all the ecozones except Atlantic Maritime, the ecozone whose variability in tree height was the most difficult to capture by our model.

5.2. Variable importance analysis

Fig. 7 depicts the variable importance for each predictor when modeling each response variable of the 6 modeled by RF in the training phase of the imputation approach. Overall, the most relevant predictors, listed by median variable importance score, are Elev, Lat, TCB, and Long. After these four, which registered importance scores for a given response variable up to 2 standard deviations above the average, there is a considerable drop in variable importance scores. When modeling response variables related to the height of the trees (elev_mean and elev_p95), the model markedly relies on Lat. Alternatively, when predicting canopy cover attributes (cover_2m and cover_mean), Elev and Long are crucial. As regards the change variables, the average importance scores for YrsSince_GrCh are decidedly larger than for Ch_attr, ultimately ranked as the least relevant variable of our set of predictors.

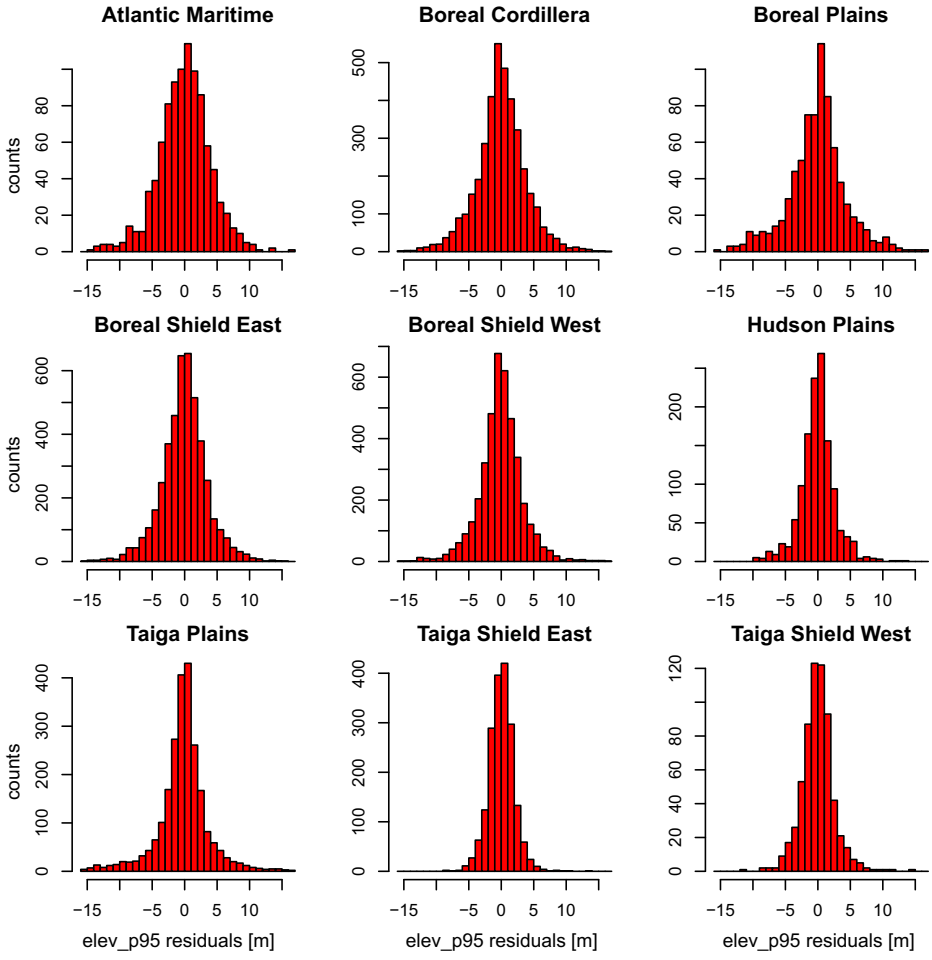

Fig. 6. Frequency distribution across the 9 sampled ecozones of the residuals (predicted minus observed values) for elev_p95 (validation set).

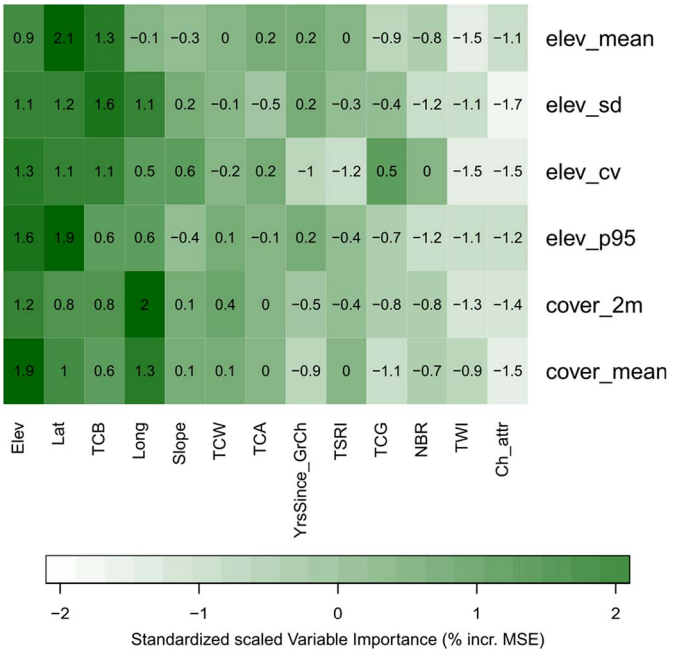

Fig. 7. Variable importance values (measured as the % increase in MSE, standardized for each response variable) for the predictors (columns sorted left to right by decreasing median importance) in each one of the 6 RF models tuned to the response variables (rows).

5.3. Forest attributes maps

The result of applying the imputation model across Canada's boreal forest is presented in Fig. 8. The central panel shows the aboveground biomass map (ag_biomass). Latitudinal trends as well as local patterns of large biomass density estimates, highlighting high-productivity regions of the boreal forest (e.g., southern areas of the Boreal Shield) are clearly visible. The top and bottom panels display some details of the boreal-wide map for the same attribute as well as for the maps of canopy height (elev_p95) and gross stem volume (stem_volume). One can appreciate the high spatial resolution of the maps revealing how the forest develops in various environments, shaped by disturbance history (see fire scar in bottom left panel or harvesting cut blocks in bottom right panel) or by local landforms (see water courses in top panel).

5.4. Average estimates per ecozone

The distribution of the estimates for gross stem volume and total aboveground biomass computed over the entirety of the treed pixels within each ecozone is shown in Fig. 9. Our predictions indicate Boreal Plains has the largest average stem_volume and ag_biomass, with 119.6 m^3/ha and 67.6 t/ha respectively, whereas the Hudson Plains present the lowest, with 40 m^3/ha and 26 t/ha, respectively. Among the most productive ecozones, we also find the Boreal Cordillera, Boreal Shield East, and Boreal Shield West.

If we consider the median value of the distributions for stem_volume and ag_biomass, there is a consistent gap between the four most productive boreal ecozones and the remainder. The Boreal Plains ecozone has the largest spread in the overall distribution of both forest attributes (standard deviation of 111.8 m^3/ha and 54.5 t/ha for stem_volume and ag_biomass, respectively), reflecting the heterogeneity of forest conditions in this part of the boreal zone.

6. Discussion

A key novelty of this research lies in the fusion of lidar plots, a means to increase the distribution and sample size of local data to inform on stand structure (Wulder et al., 2012a), with Landsat BAP composites, to map forest attributes over very large areas. The framework presented herein provides an approach to obtain wall-to-wall estimates of forest structure, resulting in a suite of otherwise unavailable information products. We anticipate these products could aid studies of the Boreal forest providing insights into forest dynamics useful for sustainable forest management and understanding climate change. The application of the developed imputation model at the scale of the Canadian boreal forest is unprecedented at a spatial resolution of 30 m, and is a major operational advance in the mapping of forest structure over large areas that leverages the benefits of two complementary remote sensing technologies. In the following sub-sections, we highlight the challenges faced in extending the mapping to the boreal level and the decisions we had to make to properly address them as well as the current limitations of the proposed methodology.

6.1. Global map accuracy in the boreal zone and comparison to other similar large-area products

For a more general comparison with other forestry studies, we refer to a meta-analysis of 81 NN-based experiments aimed at estimating growing stock volume, biomass or carbon from various sources of remotely sensed data (including a large number of studies using Landsat data) conducted by Chirici et al. (2016). The meta-analysis relied on the RMSE% to facilitate the comparison of the prediction accuracies across the different studies considered. It revealed an average RMSE% of 37%, with a standard deviation of ± 31.6% (across these types of attributes). With an RMSE% of 78.7% and 65.0% for stem_volume and ag_biomass, respectively (see Table 6), the results obtained by our RF-based imputation can be deemed as highly comparable relative to these benchmarks. Given the challenging exercise of predicting forest attributes longitudinally across an entire continent, this can be considered a promising result. Furthermore, by comparing these figures with those obtained by Zald et al. (2016), where the RMSE% for stem_volume and ag_biomass were 63.0% and 76.9% respectively, it is apparent there was no tangible loss of accuracy when extending the mapping procedure from a regional/provincial scale to the entire Canadian boreal forest.

At the national level, Beaudoin et al. (2014) reported an RMSE% of 69% for estimates of aboveground biomass derived from an imputation approach using NFI ground plots and 250 m MODIS data. This value can be compared to the overall RMSE% for aboveground biomass reported herein of 65.0%. Such a difference is notable when considering that the spatial resolution of the Beaudoin et al. (2014) estimates (250 m) is significantly coarser than that of the results reported herein (30 m). For canopy height, one of the main indicators of aboveground biomass, we compare our estimates to two maps covering the Canadian territory that have been produced by Lefsky (2010) and Simard et al. (2011) as part of their global mapping effort. A thorough assessment of these GLAS-based products has been carried out in Bolton et al. (2013) on the same nationwide lidar transect we used to calibrate our forest structure models. As reported by Bolton et al. (2013), the average RMSE values across the considered ecozones were 7.4 (Lefsky, 2010) and 3.9 m (Simard et al., 2011). While not entirely comparable, our elev_p95 estimates had a global RMSE of 3.56 m, a more accurate result, especially if we consider the averaging effect induced by the spatial unit (925-m cell) used for the assessment of the maps produced by Lefsky (2010) and Simard et al. (2011).

6.2. Map accuracy in each ecozone and comparison of average estimates

The variations in structure that exist across the boreal forest explain the difficulty in accurately predicting the forest attributes with a single model. High variability in canopy height across the ecozones is visible in Fig. 3 and, can be related to the R^2 barplots of Fig. 5 and to the plots of the residuals of Fig. 6. Indeed, the ecozones that are more difficult to

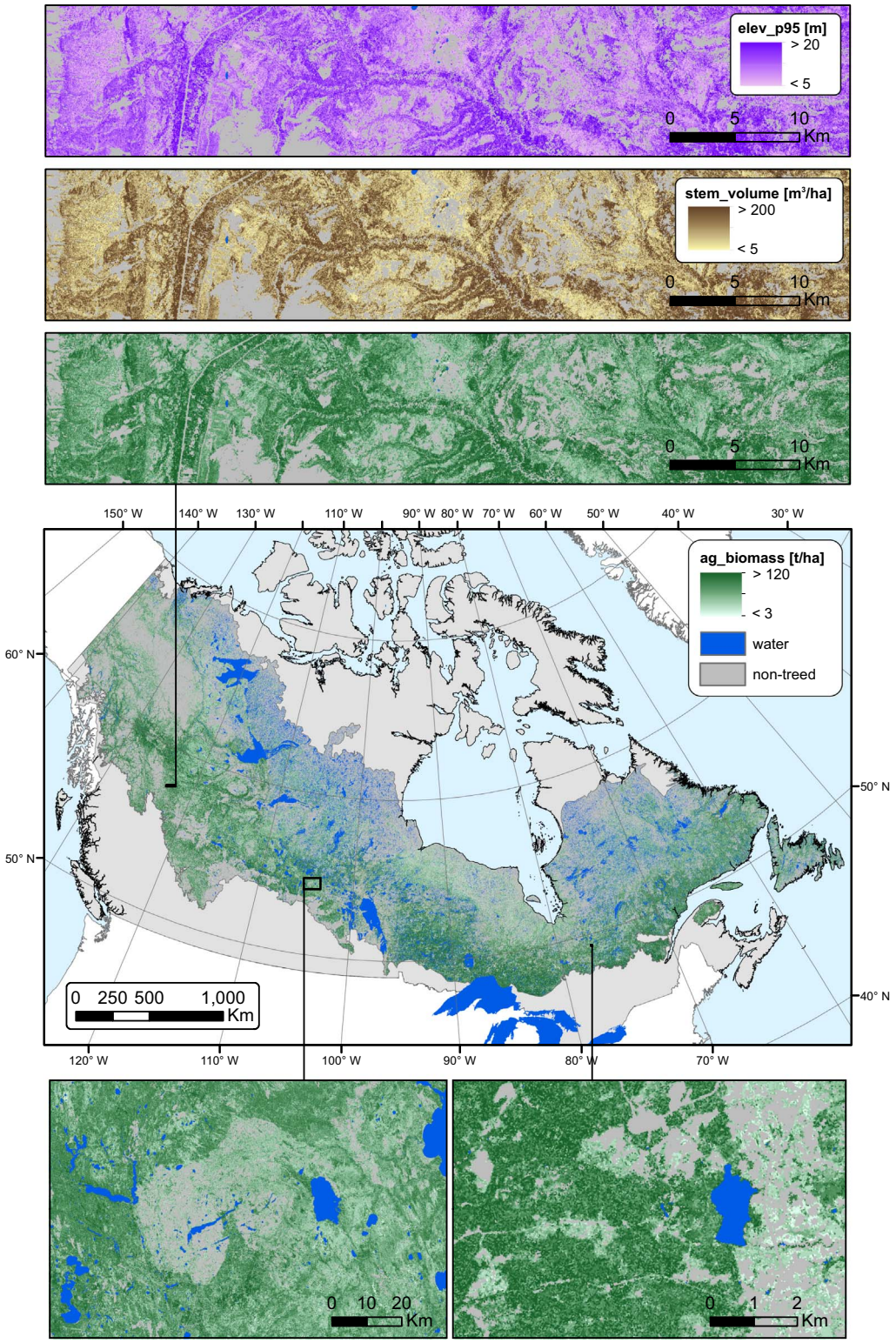

Fig. 8. 30-m spatial resolution maps for the year 2010. Center: map of ag_biomass (total aboveground biomass in t/ha) in the boreal forest of Canada (color scale applies to all ag_biomass map details). Top: map detail for elev_p95 (95th percentile of first returns height in m), stem_volume (gross stem volume in m^3/ha) and ag_biomass on a sub-region in northern British Columbia with a landscape shaped by water courses. Bottom: ag_biomass map detail on sub-regions in (left) central Saskatchewan showing fire scars and in (right) western Quebec with clearly visible harvesting cut blocks.

appropriately model (i.e., $R^2 < 0.3$ for height, volume, and biomass) are Atlantic Maritime and Taiga Shield West, two ecozones that displayed either very large or very small tree height values. Especially the Atlantic Maritime ecozone is critical to capture with a global model because of the different forest conditions encountered therein, particularly the mild climate and diversity in forest types. Additionally, only a relatively small portion of the lidar transects covers the zone, leading to fewer samples coming from this area.

The reasons for the best performances being observed in the Taiga Plains, Boreal Plains and Boreal Cordillera ecozones are less clear.

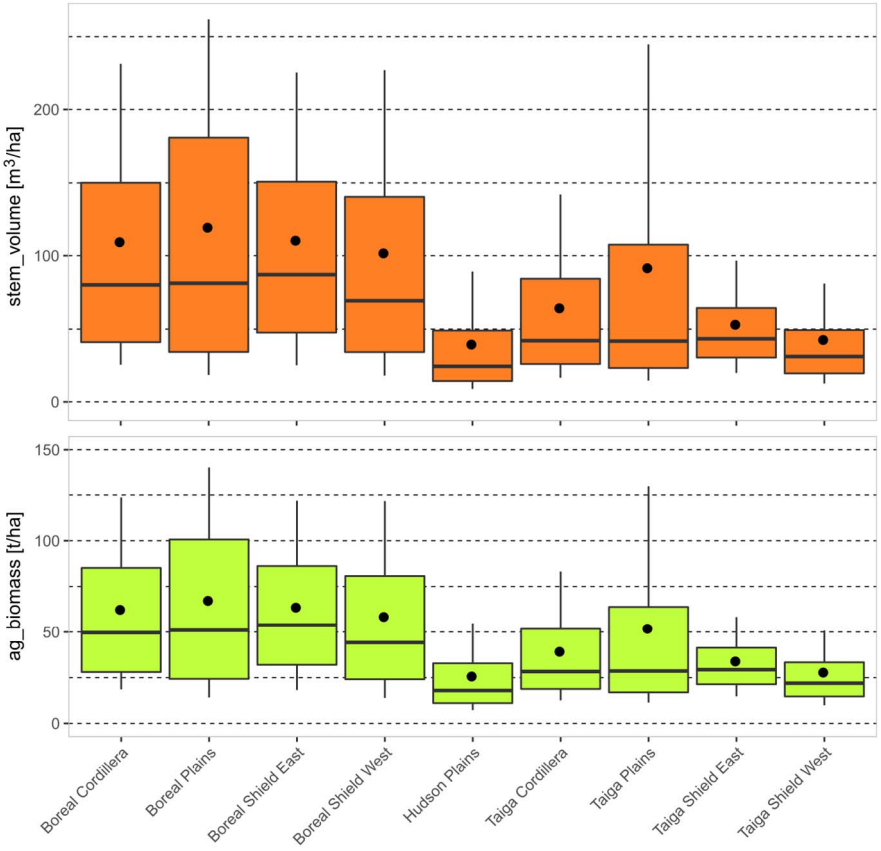

Fig. 9. Boxplots of the distribution in each ecozone of (top) gross stem volume (stem_volume in m^3/ha) and (bottom) total aboveground biomass (ag_biomass in t/ha). Whiskers denote the 10th and 90th centiles of the distribution. Mean values are shown with black circles.

Given the diversity of forest conditions and variability in sample sizes for each ecozone, caution must be exercised when interpreting small differences in model accuracy. Also, we point out that the transects themselves were not optimized to be representative of within-ecozone conditions but dictated by a range of factors (from spatial coverage aims to practical considerations such as airport locations, runway conditions, fuel availability and maintained schedules, as per Wulder et al., 2012a, 2012b).

Our mean aboveground biomass estimates for each terrestrial ecozone (denoted by circles in Fig. 9) generally agree with the values reported by the Canadian NFI (https://nfi.nfis.org/en/customized_report, statistics for "forest land"). Taiga Cordillera and Taiga Plains, with a reference biomass values of 76.7 t/ha and 82.7 t/ha, respectively, are the only ecozones where our estimated mean values markedly differ: 39.6 t/ha and 52.2 t/ha, respectively. The reference values in rest of the inventoried ecozones we considered are more closely matching the NFI figures: Boreal Cordillera 70.9 (NFI's estimate) vs. 62.6 t/ha (our estimate), Boreal Plains 75.9 vs. 67.6 t/ha, Boreal Shield 76.5 vs. 58.7 (Boreal Shield West) or 63.8 t/ha (Boreal Shield East), Hudson Plains 22.5 vs. 26.0 t/ha, Taiga Shield 48.5 vs. 34.3 (Taiga Shield East) or 28.2 t/ha (Taiga Shield West). The general match between the outputs of our model and these reference estimates confirms the validity of our approach.

6.3. Relevance of the types of predictor variables

In the variable importance results presented in Section 5.2, the considerable relevance of predictors describing the geographical position of the plots in the three dimensions is noteworthy. Elevation above sea level (Elev) plays an important role in our model because it provides a continuous variable that characterizes the change in forest conditions as a function of the altitude above sea level. Likewise, the spatial coordinates, longitude (Long) and latitude (Lat), capture large-area trends in temperature gradients, growing season length, and productivity.

In addition to the broad-scale patterns captured by elevation, latitude, and longitude, fine-scale spatial information is needed to generate accurate high-resolution maps of forest structure. To this end, the spectral indices derived from Landsat pixel composites were crucial for the mapping. The Tasseled Cap components, in particular the brightness component (TCB), were important in the modeling of every lidar metric considered in this study. The use of this type of spectral data in such a large-area mapping task was enabled by the latest developments in BAP compositing techniques combined with the opening of the Landsat archive. Looking forward, the integration of Landsat Operational Land Imager (OLI) data, being acquired starting from 2013, will improve the availability of cloud-free scenes (Roy et al., 2014), hence reducing compositing artifacts. Similarly, due to its comparable spectral characteristics and spatial resolution, Sentinel-2 data could also be considered as a viable source of spectral information (Drusch et al., 2012). The addition of topographic variables (e.g., slope, the 5th most important predictor overall) further informs on site properties, enabling a model that captured local variation in canopy structure, yielding meaningful forest attributes maps.

We found that the time since largest change for a given pixel (YrsSince_GrCh) is also important in many models, a confirmation that the inclusion of such a temporal indicator is relevant to capture forest regrowth patterns. Indeed, the more years since a significant disturbance event have passed, the more advanced the recovery of the forest stand will be (Bartels et al., 2016). This effect was particularly marked for response variables related to the height of the canopy (see elev_p95, elev_mean and elev_sd in Fig. 7). Conversely, the type of change (Ch_attr) does not prove to be that important in the RF models,

being ranked last. Indeed, the vast majority of the sampled plots (90.6%) have never experienced a disturbance in the monitored period, thus limiting the number of instances where such a change variable can impact the modeling. Of note, the inclusion of time since disturbance and change type allowed us to maintain the same model accuracy of Zald et al. (2016), whose model used a larger number of change variables (e.g., spectral magnitude of the changes).

6.4. Challenges posed by the large-area mapping of forest structure

The extension of the regional imputation model prototyped by Zald et al. (2016) to a boreal-wide implementation involved a number of crucial decisions to address the challenges associated with a large-area application. We list and discuss these below with the purpose of providing insights for those aiming to implement similar applications of wall-to-wall forest structure mapping:

1. Single global model vs. multiple ecozone-level models
2. Availability and coverage of lidar data
3. Spatial invariance of the surface reflectance pixel composites
4. Modeling approach: imputation vs. prediction
5. Choice of response variables to model
6. Data processing architecture.

Firstly, a crucial factor to consider is the number of distinct forested ecological domains mapped, which in this study included nine ecozones, extending west to east across the North American continent, compared to the portions of three ecozones mapped by Zald et al. (2016). Differences in vegetative ecosystems require the applied model to capture and differentiate several types of local forest conditions. One option to handle such heterogeneity could be to consider each ecozone separately by building individual imputation models rather than a single global model. However, in our framework, we used a global model to avoid boundary effects when adjacent pixels are predicted at the interface between two ecozones by two different models. Moreover, our lidar transects do not provide for a representative sample within each ecozone. To account for these local ecological conditions, which are driven by factors such as temperature, precipitation and continentality, we decided to include the geographic coordinates of the samples (latitude and longitude) as predictor variables to inform the model. This ensured the model relied more heavily on plots located in the same geographical area when imputing values at a given mapping location, resulting in a local model better capturing the forest conditions in each ecozone. Such an idea is taken from the field of geostatistcs and accounts for spatial autocorrelation among the response variables (Matheron, 1963).

The spatial representativeness of the lidar data is an important criterion for the generation of locally accurate maps of forest attributes. When moving from regional predictions to predictions undertaken across much broader geographic and environmental domains, the availability of consistent lidar-derived plots is a key factor for model development. In our case, the lidar transect data acquired in the 2010 national campaign spans an area that closely matches the region of interest for this study: the Canadian boreal zone. In the imputation process, when imputing values in a given sub-region of the boreal forest, suitable donor plots from reasonably comparable forest conditions could always be found (with the exception of the ecozones Atlantic Maritime and Taiga Shield West, see Fig. 5). Moreover, the lidar plots represented the broad range of forest structural conditions present in the boreal forest. This representativeness is critical for an imputation approach, which cannot extrapolate beyond the range of conditions present in the calibration data used in model development.

Spectrally consistent and spatially comprehensive optical data is the other essential condition for a large-area mapping effort. In fact, robust surface reflectance image composites are key to ensuring that stands with similar characteristics across the mapped area also present similar associated spectral values. For Landsat imagery, this transformation to surface reflectance is currently implemented as an analysis-ready data product by the USGS. This ease of access to high-quality optical products opens opportunities for mapping projects covering large surfaces in any part of the world. To consistently map forest attributes in space, besides the physically-based transformation from digital numbers to surface reflectance values, additional steps are required to obtain the spatial/temporal coverage required by the application. The BAP and temporal interpolation approaches used to composite and fill gaps in the image time-series (Hermosilla et al., 2015a) are effective and are largely applicable across the global terrestrial ecosphere, given caveats on spatial and temporal coverage of archival data (Wulder et al., 2016).

In terms of type of statistical model to apply, when mapping multiple attributes at the same time, two main options can be considered: an imputation approach (one single model for all of the response variables) or a parametric/non-parametric regression approach (whereby a separate model is generated per response variable). The challenge one faces with the imputation is that the model is more constrained when assigning a value to a new mapping location. It will be bound to selecting the plot that best fits, on average, a number of response variables at a time. In the latter case, instead, the focus is on one single attribute only and the model can provide a solution optimized to explain the variance of each response variable. The advantage of the imputation approach is that one will map consistent and realistic forest conditions, as all the attributes describing a patch of forest are assigned as a set. Critically, as demonstrated in Zald et al. (2016), the lidar metrics themselves can be imputed, providing flexibility for model refinement and/or other modeling applications (as new models can be applied to mapped metrics directly). Maintenance of the covariance structure between variables is another advantage of the imputation approach, although often coming at the cost of lower model accuracy.

Closely linked to the selection of the modeling approach is the choice of the attributes one wants to include in the mapping process, especially when using an imputation model. Indeed, the subset of response variables to model has to appropriately capture the forest conditions one is interested in. They should be measurements that are consistent across all the sub-regions included in the sampling/mapping task and should not be subject to noise contaminations or to uncertainties deriving from another modeling process. In our study, we focused on the lidar metrics in this phase and attached as ancillary variables the actual derived forest attributes. In other words, the imputation is guided by the structural metrics derived from lidar. The forest attributes of interest (basal area, biomass, volume, Lorey's height) are carried as ancillary variables in the plot matching process, as per Zald et al. (2016).

Any large-area mapping task requires massive amounts of geospatial data. Thus, defining an appropriate data processing scheme is a major challenge to ensure the robustness and efficiencies of the mapping task. A tile-based approach that partitions the area of interest into manageable units (i.e. to avoid memory issues and computational limitations) is often required. Access to advanced computing facilities that provide for a large number of parallel processing tasks, is also advantageous. In our case, we partition our large study area, which spanned longitudinally the North-American continent, into UTM zone tiles, thereby maximizing the memory potential offered by the local and remote high performance computing facilities utilized.

6.5. Limitations of the imputation mapping across the boreal zone

One limitation of our study concerns the data source for the derived forest attributes. Indeed, as mentioned in Section 3.1, the input values for our model for the response variables Lorey's tree height (loreys_height), basal area (basal_area), gross stem volume (stem_volume) and total aboveground biomass (ag_biomass), are themselves the result of a modeling process by linear regression based on field plots (Wulder et al., 2012a). The accuracy of such predictions ranges from 0.64 to

0.83 R^2. For this reason, the accuracy metrics presented in this paper for the four forest attributes are to be interpreted with caution, similar to forest inventory data where visually interpreted polygons are the basis for look-up table based estimates of unmeasured attributes.

Another source of error in our estimates of forest attributes is related to our predictions being independent of species. The issue of including species within structural based predictions is complex, with species influencing wood density and structure of the canopy which, in turn, impact biomass (Lambert et al., 2005). However, previous work has highlighted that, at least for estimating tree volume, precise canopy height measurements are more crucial than species knowledge (Tompalski et al., 2014), and presently, no detailed species information is available at a commensurate resolution.

6.6. Temporal extension of the model

The study presented herein opens future research opportunities for a temporal extension of the predictions made by the current model. The temporal transferability of single year imputation models has been suggested in Deo et al. (2017); Fekety et al. (2014) and offers promise for the estimation of forest growth and development over time, with research required to incorporate appropriate successional insights, such as availing upon forestry growth and yield experience.

To enable this temporal extension, on the one hand, the current Landsat BAP composites time-series and derived change products covering the period from 1984 to 2012 can be extended with new data from the OLI sensor onboard Landsat 8 (Hermosilla et al., 2017). On the other hand, an improved understanding of Landsat Multispectral Scanner System (MSS) radiometry and its subsequent integration in the C2C routines may allow for further extension back in time prior to 1984 (Braaten et al., 2015; Pflugmacher et al., 2012).

7. Conclusions

Detailed, spatially explicit maps of forest structure over large areas are increasingly required to support science, policy, and reporting information requirements. In this research, we demonstrated the opportunities and challenges associated with the synergistic use of Landsat and lidar data to map forest structural attributes across Canada's boreal forest representing 2010 conditions. We investigated the use of wall-to-wall Landsat surface reflectance pixel composites and their associated spectral and change-related features to extrapolate over the entire Canadian boreal zone a set of lidar metrics and derived forest attributes utilizing a > 25,000 km boreal-wide transect of airborne lidar data. These records of forest structure and aboveground biomass, summarized on a grid of lidar plots, have been mapped for the area with a NN imputation approach that uses RF as base method to relate response variables to the spatially comprehensive set of predictor variables. Promising goodness of fit statistics were obtained when validating the predictions globally in the boreal forest and at the ecozone level. Concurrently, we undertook a variable importance analysis to gain insights into the driving factors in our predictions, allowing us to determine the relevance of positional and elevation attributes, when combined with Landsat-derived spectral indices and disturbance-related metrics. Our resulting outputs yielded reliable estimates of the average aboveground biomass (26–67.6 t/ha) and gross stem volume (40–119.6 m^3/ha) available within each of the boreal ecozones, which were previously unavailable from data at a 30-m spatial resolution. The results presented in this research indicate the utility of lidar-sample supported mapping of forest structural attributes over large areas using optical satellite data, such as Landsat, with opportunity indicated for Sentinel-2. The geospatial layers produced provide spatially consistent, transparent and accurate data regarding key forest structure attributes suitable to be integrated in large-area forest inventory and monitoring efforts.

Acknowledgments

This research was undertaken as part of the “National Terrestrial Ecosystem Monitoring System (NTEMS): Timely and detailed national cross-sector monitoring for Canada” project jointly funded by the Canadian Space Agency (CSA), Government Related Initiatives Program (GRIP), and the Canadian Forest Service (CFS) of Natural Resources Canada. This research was enabled in part by support provided by WestGrid (www.westgrid.ca) and Compute Canada (www.computecanada.ca). This work has also been supported by a mobility grant offered by the University of Lausanne, Switzerland, for the project titled: “Fusion of lidar and optical remote sensing data for forestry applications: a machine learning approach”. The authors thank Dr. Douglas Bolton for the fruitful discussions had throughout the study. We also thank the two anonymous reviewers for their helpful suggestions on earlier versions of this paper.

References

Ahmed, O.S., Franklin, S.E., Wulder, M.A., White, J.C., 2015. Characterizing stand-level forest canopy cover and height using Landsat time series, samples of airborne LiDAR, and the random forest algorithm. ISPRS J. Photogramm. Remote Sens. 101, 89–101.

Baltsavias, E.P., 1999. Airborne laser scanning: basic relations and formulas. ISPRS J. Photogramm. Remote Sens. 54, 199–214.

Bartels, S.F., Chen, H.Y.H.H., Wulder, M.A., White, J.C., 2016. Trends in post-disturbance recovery rates of Canada's forests following wildfire and harvest. For. Ecol. Manag. 361, 194–207. http://dx.doi.org/10.1016/j.foreco.2015.11.015.

Bater, C.W., Wulder, M.A., Coops, N.C., Hopkinson, C., Coggins, S.B., Arsenault, E., Beaudoin, A., Guindon, L., Hall, R.J., Villemaire, P., Woods, M., 2011. Model Development for the Estimation of Aboveground Biomass Using a Lidar-Based Sample of Canada's Boreal Forest, SilviLaser 2011. Hobart, Tasmania, Australia.

Beaudoin, A., Bernier, P.Y., Guindon, L., Villemaire, P., Guo, X.J., Stinson, G., Bergeron, T., Magnussen, S., Hall, R.J., 2014. Mapping attributes of Canada's forests at moderate resolution through kNN and MODIS imagery. Can. J. For. Res. 44, 521–532. http://dx.doi.org/10.1139/cjfr-2013-0401.

Belgiu, M., Drăgu, L., 2016. Random forest in remote sensing: a review of applications and future directions. ISPRS J. Photogramm. Remote Sens. 114, 24–31. http://dx.doi.org/10.1016/j.isprsjprs.2016.01.011.

Beven, K.J., Kirkby, M.J., 1979. A physically based, variable contributing area model of basin hydrology. Hydrol. Sci. J. 24, 43–69.

Bolton, D.K., Coops, N.C., Wulder, M.A., 2013. Investigating the agreement between global canopy height maps and airborne Lidar derived height estimates over Canada. Can. J. Remote. Sens. 39, S139–S151.

Boudreau, J., Nelson, R.F., Margolis, H.A., Beaudoin, A., Guindon, L., Kimes, D.S., 2008. Regional aboveground forest biomass using airborne and spaceborne LiDAR in Québec. Remote Sens. Environ. 112, 3876–3890. http://dx.doi.org/10.1016/j.rse.2008.06.003.

Braaten, J.D., Cohen, W.B., Yang, Z., 2015. Automated cloud and cloud shadow identification in Landsat MSS imagery for temperate ecosystems. Remote Sens. Environ. 169, 128–138. http://dx.doi.org/10.1016/j.rse.2015.08.006.

Brandt, J.P., 2009. The extent of the North American boreal zone. Environ. Rev. 17, 101–161.

Brandt, J.P., Flannigan, M.D., Maynard, D.G., Thompson, I.D., Volney, W.J.A., 2013. An introduction to Canada's boreal zone: ecosystem processes, health, sustainability, and environmental issues. Environ. Rev. 21, 207–226.

Breiman, L., 2001. Random forests. Mach. Learn. 45, 5–32.

Brosofske, K.D., Froese, R.E., Falkowski, M.J., Banskota, A., 2014. A review of methods for mapping and prediction of inventory attributes for operational forest management. For. Sci. 60, 733–756. http://dx.doi.org/10.5849/forsci.12-134.

Canadian Council of Forest Ministers, 1995. Defining Sustainable Forest Management: A Canadian Approach to Criteria and Indicators. Canadian Council of Forest Ministers by Canadian Forest Service, Natural Resources Canada.

Chen, G., Wulder, M.A., White, J.C., Hilker, T., Coops, N.C., 2012. Lidar calibration and validation for geometric-optical modeling with Landsat imagery. Remote Sens. Environ. 124, 384–393. http://dx.doi.org/10.1016/j.rse.2012.05.026.

Chirici, G., Mura, M., McInerney, D., Py, N., Tomppo, E.O., Waser, L.T., Travaglini, D., McRoberts, R.E., 2016. A meta-analysis and review of the literature on the k-Nearest Neighbors technique for forestry applications that use remotely sensed data. Remote Sens. Environ. 176, 282–294.

Cohen, W.B., Goward, S.N., 2004. Landsat's role in ecological applications of remote sensing. Bioscience 54, 535–545.

Cohen, W.B., Maiersperger, T.K., Spies, T.A., Oetter, D.R., 2001. Modelling forest cover attributes as continuous variables in a regional context with Thematic Mapper data. Int. J. Remote Sens. 22, 2279–2310.

Crist, E.P., Cicone, R.C., 1984. Application of the tasseled cap concept to simulated thematic mapper data. Photogramm. Eng. Remote. Sens. 50, 343–352.

Crookston, N.L., Finley, A.O., 2008. yaImpute: an R package for kNN imputation. J. Stat. Softw. 23, 1–16.

Deo, R.K., Russell, M.B., Domke, G.M., Woodall, C.W., Falkowski, M.J., Cohen, W.B., 2017. Using Landsat time-series and LiDAR to inform aboveground forest biomass

baselines in Northern Minnesota, USA. Can. J. Remote. Sens. 43, 28–47. http://dx.doi.org/10.1080/07038992.2017.1259556.
Draper, N.R., Smith, H., 1998. Applied Regression Analysis. John Wiley & Sons.
Drusch, M., Del Bello, U., Carlier, S., Colin, O., Fernandez, V., Gascon, F., Hoersch, B., Isola, C., Laberinti, P., Martimort, P., Meygret, A., 2012. Sentinel-2: ESA's optical high-resolution mission for GMES operational services. Remote Sens. Environ. 120, 25–36.
Duane, M.V., Cohen, W.B., Campbell, J.L., Hudiburg, T., Turner, D.P., Weyermann, D.L., 2010. Implications of alternative field-sampling designs on Landsat-based mapping of stand age and carbon stocks in Oregon forests. For. Sci. 56, 405–416.
Duncanson, L.I., Niemann, K.O., Wulder, M.A., 2010. Integration of GLAS and Landsat TM data for aboveground biomass estimation. Can. J. Remote. Sens. 36, 129–141. http://dx.doi.org/10.5589/m10-037.
Ecological Stratification Working Group, 1996. A National Ecological Framework for Canada. Environment Conservation Service, Environment Canada, Ottawa. http://ecozones.ca/.
Eskelson, B.N.I., Temesgen, H., Lemay, V., Barrett, T.M., Crookston, N.L., Hudak, A.T., 2009. The roles of nearest neighbor methods in imputing missing data in forest inventory and monitoring databases. Scand. J. For. Res. 24, 235–246. http://dx.doi.org/10.1080/02827580902870490.
Fekety, P. a, Falkowski, M.J., Hudak, A.T., 2014. Temporal transferability of LiDAR-based imputation of forest inventory attributes. Can. J. For. Res. 45, 422–435. http://dx.doi.org/10.1139/cjfr-2014-0405.
Franklin, J., Rogan, J., Phinn, S.R., Woodcock, C.E., 2003. Rationale and conceptual framework for classification approaches to assess forest resources and properties. In: Wulder, M.A., Franklin, S.E. (Eds.), Remote Sensing of Forest Environments: Concepts and Case Studies. Springer, US, Boston, MA, pp. 279–300. http://dx.doi.org/10.1007/978-1-4615-0306-4_10.
Frazier, R.J., Coops, N.C., Wulder, M.A., Kennedy, R., 2014. Characterization of aboveground biomass in an unmanaged boreal forest using Landsat temporal segmentation metrics. ISPRS J. Photogramm. Remote Sens. 92, 137–146. http://dx.doi.org/10.1016/j.isprsjprs.2014.03.003.
Gao, X., Huete, A.R., Ni, W., Miura, T., 2000. Optical-biophysical relationships of vegetation spectra without background contamination. Remote Sens. Environ. 74, 609–620.
Gillis, M.D., Omule, A.Y., Brierley, T., 2005. Monitoring Canada's forests: the national forest inventory. For. Chron. 81, 214–221.
Gislason, P.O., Benediktsson, J.A., Sveinsson, J.R., 2006. Random forests for land cover classification. Pattern Recogn. Lett. 27, 294–300.
Gleason, C.J., Im, J., 2012. Forest biomass estimation from airborne LiDAR data using machine learning approaches. Remote Sens. Environ. 125, 80–91.
Hansen, M.C., Loveland, T.R., 2012. A review of large area monitoring of land cover change using Landsat data. Remote Sens. Environ. 122, 66–74.
Hansen, M.C., Potapov, P.V., Goetz, S.J., Turubanova, S., Tyukavina, A., Krylov, A., Kommareddy, A., Egorov, A., 2016. Mapping tree height distributions in Sub-Saharan Africa using Landsat 7 and 8 data. Remote Sens. Environ. 185, 221–232. http://dx.doi.org/10.1016/j.rse.2016.02.023.
Henderson, E.B., Ohmann, J.L., Gregory, M.J., Roberts, H.M., Zald, H.S.J., 2014. Species distribution modelling for plant communities: stacked single species or multivariate modelling approaches? Appl. Veg. Sci. 17, 516–527.
Hermosilla, T., Wulder, M.A., White, J.C., Coops, N.C., Hobart, G.W., 2015a. Regional detection, characterization, and attribution of annual forest change from 1984 to 2012 using Landsat-derived time-series metrics. Remote Sens. Environ. 170, 121–132.
Hermosilla, T., Wulder, M.A., White, J.C., Coops, N.C., Hobart, G.W., 2015b. An integrated Landsat time series protocol for change detection and generation of annual gap-free surface reflectance composites. Remote Sens. Environ. 158, 220–234.
Hermosilla, T., Wulder, M.A., White, J.C., Coops, N.C., Hobart, G.W., Campbell, L.B., 2016. Mass data processing of time series Landsat imagery: pixels to data products for forest monitoring. Int. J. Digital Earth 9, 1035–1054.
Hermosilla, T., Wulder, M.A., White, J.C., Coops, N.C., Hobart, G.W., 2017. Updating Landsat time series of surface-reflectance composites and forest change products with new observations. Int. J. Appl. Earth Obs. Geoinf. 63, 104–111. http://dx.doi.org/10.1016/j.jag.2017.07.013.
Hermosilla, T., Wulder, M.A., White, J.C., Coops, N.C., Hobart, G.W., 2018. Disturbance-informed annual land cover classification maps of Canada for a 29-year Landsat time series. Can. J. Remote Sens.
Huang, S., Ramirez, C., Conway, S., Kennedy, K., Kohler, T., Liu, J., 2017. Mapping site index and volume increment from forest inventory, Landsat, and ecological variables in Tahoe National Forest, California, USA. Can. J. For. Res. 47, 113–124.
Hudak, A.T., Lefsky, M.A., Cohen, W.B., Berterretche, M., 2002. Integration of lidar and Landsat ETM+ data for estimating and mapping forest canopy height. Remote Sens. Environ. 82, 397–416.
Hudak, A.T., Crookston, N.L., Evans, J.S., Hall, D.E., Falkowski, M.J., 2008. Nearest neighbor imputation of species-level, plot-scale forest structure attributes from LiDAR data. Remote Sens. Environ. 112, 2232–2245.
Huete, A.R., Liu, H.Q., Batchily, K. v, Van Leeuwen, W., 1997. A comparison of vegetation indices over a global set of TM images for EOS-MODIS. Remote Sens. Environ. 59, 440–451.
Ji, L., Gallo, K., 2006. An agreement coefficient for image comparison. Photogramm. Eng. Remote. Sens. 72, 823–833.
Ju, J., Masek, J.G., 2016. The vegetation greenness trend in Canada and US Alaska from 1984–2012 Landsat data. Remote Sens. Environ. 176, 1–16.
Kauth, R.J., Thomas, G.S., 1976. The tasselled cap-a graphic description of the spectral-temporal development of agricultural crops as seen by Landsat. In: LARS Symposia, pp. 159.
Key, C.H., Benson, N.C., 2005. Landscape Assessment: Remote Sensing of Severity, the Normalized Burn Ratio and Ground Measure of Severity, the Composite Burn Index, FIREMON: Fire Effects Monitoring and Inventory System Ogden. USDA Forest Service, Rocky Mountain Res. Station, Utah.
Kurz, W.A., Apps, M.J., 1999. A 70-year retrospective analysis of carbon fluxes in the Canadian forest sector. Ecol. Appl. 9, 526–547.
Lambert, M.C., Ung, C.H., Raulier, F., 2005. Canadian national tree aboveground biomass equations. Can. J. For. Res. 35, 1996–2018.
Latifi, H., Nothdurft, A., Koch, B., 2010. Non-parametric prediction and mapping of standing timber volume and biomass in a temperate forest: application of multiple optical/LiDAR-derived predictors. Forestry 83, 395–407.
Lefsky, M.A., 2010. A global forest canopy height map from the moderate resolution imaging spectroradiometer and the geoscience laser altimeter system. Geophys. Res. Lett. 37.
Lefsky, M.A., Turner, D.P., Guzy, M., Cohen, W.B., 2005. Combining lidar estimates of aboveground biomass and Landsat estimates of stand age for spatially extensive validation of modeled forest productivity. Remote Sens. Environ. 95, 549–558.
Liaw, A., Wiener, M., 2002. Classification and regression by random Forest. In: R News. 2. pp. 18–22.
Lu, D., 2005. Aboveground biomass estimation using Landsat TM data in the Brazilian Amazon. Int. J. Remote Sens. 26, 2509–2525.
Lu, D., 2006. The potential and challenge of remote sensing-based biomass estimation. Int. J. Remote Sens. 27, 1297–1328.
Margolis, H.A., Nelson, R.F., Montesano, P.M., Beaudoin, A., Sun, G., Andersen, H.-E., Wulder, M.A., 2015. Combining satellite lidar, airborne lidar, and ground plots to estimate the amount and distribution of aboveground biomass in the boreal forest of North America. Can. J. For. Res. 45, 838–855. http://dx.doi.org/10.1139/cjfr-2015-0006.
Masek, J.G., Vermote, E.F., Saleous, N.E., Wolfe, R., Hall, F.G., Huemmrich, K.F., Gao, F., Kutler, J., Lim, T.-K., 2006. A Landsat surface reflectance dataset for North America, 1990–2000. IEEE Geosci. Remote Sens. Lett. 3, 68–72.
Matheron, G., 1963. Principles of geostatistics. Econ. Geol. 58, 1246–1266.
McGaughey, R.J., 2013. FUSION/LDV: Software for LIDAR Data Analysis and Visualization. US Department of Agriculture, Forest Service, Pacific Northwest Research Station, Seattle, WA.
Moeur, M., Stage, A.R., 1995. Most similar neighbor: an improved sampling inference procedure for natural resource planning. For. Sci. 41, 337–359.
Natural Resources Canada, 2016. The state of Canada's forests. Annu. Rep. 2016.
Neigh, C.S.R., Nelson, R.F., Ranson, K.J., Margolis, H.A., Montesano, P.M., Sun, G., Kharuk, V., Næsset, E., Wulder, M.A., Andersen, H.E., 2013. Taking stock of circumboreal forest carbon with ground measurements, airborne and spaceborne LiDAR. Remote Sens. Environ. 137, 274–287. http://dx.doi.org/10.1016/j.rse.2013.06.019.
Nelson, R., 2013. How did we get here? An early history of forestry lidar. Can. J. Remote Sens. 39, S6–S17. http://dx.doi.org/10.5589/m13-011.
Nelson, R., Margolis, H., Montesano, P., Sun, G., Cook, B., Corp, L., Andersen, H.E., DeJong, B., Pellat, F.P., Fickel, T., Kauffman, J., Prisley, S., 2017. Lidar-based estimates of aboveground biomass in the continental US and Mexico using ground, airborne, and satellite observations. Remote Sens. Environ. 188, 127–140. http://dx.doi.org/10.1016/j.rse.2016.10.038.
Ohmann, J.L., Gregory, M.J., 2002. Predictive mapping of forest composition and structure with direct gradient analysis and nearest-neighbor imputation in coastal Oregon, USA. Can. J. For. Res. 32, 725–741.
Pflugmacher, D., Cohen, W.B., Kennedy, R.E., 2012. Using Landsat-derived disturbance history (1972–2010) to predict current forest structure. Remote Sens. Environ. 122, 146–165. http://dx.doi.org/10.1016/j.rse.2011.09.025.
Potapov, P., Turubanova, S., Hansen, M.C., 2011. Regional-scale boreal forest cover and change mapping using Landsat data composites for European Russia. Remote Sens. Environ. 115, 548–561.
Powell, S.L., Cohen, W.B., Yang, Z., Pierce, J.D., Alberti, M., 2008. Quantification of impervious surface in the Snohomish water resources inventory area of western Washington from 1972-2006. Remote Sens. Environ. 112, 1895–1908.
Powell, S.L., Cohen, W.B., Healey, S.P., Kennedy, R.E., Moisen, G.G., Pierce, K.B., Ohmann, J.L., 2010. Quantification of live aboveground forest biomass dynamics with Landsat time-series and field inventory data: a comparison of empirical modeling approaches. Remote Sens. Environ. 114, 1053–1068.
Roberts, D.W., Cooper, S.V., 1989. Concepts and Techniques of Vegetation Mapping.
Roy, D.P., Ju, J., Kline, K., Scaramuzza, P.L., Kovalskyy, V., Hansen, M., Loveland, T.R., Vermote, E., Zhang, C., 2010. Web-enabled Landsat Data (WELD): Landsat ETM+ composited mosaics of the conterminous United States. Remote Sens. Environ. 114, 35–49.
Roy, D.P., Wulder, M.A., Loveland, T.R., Woodcock, C.E., Allen, R.G., Anderson, M.C., Helder, D., Irons, J.R., Johnson, D.M., Kennedy, R., et al., 2014. Landsat 8: science and product vision for terrestrial global change research. Remote Sens. Environ. 145, 154–172.
Simard, M., Pinto, N., Fisher, J.B., Baccini, A., 2011. Mapping forest canopy height globally with spaceborne lidar. J. Geophys. Res. Biogeosciences 116, 1–12. http://dx.doi.org/10.1029/2011JG001708.
Tachikawa, T., Kaku, M., Iwasaki, A., Gesch, D.B., Oimoen, M.J., Zhang, Z., Danielson, J.J., Krieger, T., Curtis, B., Haase, J., Abrams, M., 2011. ASTER Global Digital Elevation Model Version 2-Summary of Validation Results.
Tompalski, P., Coops, N.C., White, J.C., Wulder, M.A., 2014. Simulating the impacts of error in species and height upon tree volume derived from airborne laser scanning data. For. Ecol. Manag. 327, 167–177.
Tomppo, E., Olsson, H., Ståhl, G., Nilsson, M., Hagner, O., Katila, M., 2008. Combining national forest inventory field plots and remote sensing data for forest databases.

Remote Sens. Environ. 112, 1982–1999.
Tomppo, E., Gschwantner, T., Lawrence, M., McRoberts, R.E., Gabler, K., Schadauer, K., Vidal, C., Lanz, A., Ståhl, G., Cienciala, E., 2010. National forest inventories. In: Pathways Common Reporting. Eur. Sci. Found, pp. 541–553.
Wang, X., Huang, H., Gong, P., Biging, G.S., Xin, Q., Chen, Y., Yang, J., Liu, C., 2016. Quantifying multi-decadal change of planted forest cover using airborne LiDAR and Landsat imagery. Remote Sens. 8, 62.
White, J.C., Wulder, M.A., Varhola, A., Vastaranta, M., Coops, N.C., Cook, B.D., Pitt, D., Woods, M., 2013. A Best Practices Guide for Generating Forest Inventory Attributes from Airborne Laser Scanning Data Using an Area-Based Approach, Information Report FI-X-10. Canadian Forest Service, Canadian Wood Fibre Centre, Pacific Forestry Centre, Victoria, B.C.
White, J.C., Wulder, M.A., Hobart, G.W., Luther, J.E., Hermosilla, T., Griffiths, P., Coops, N.C., Hall, R.J., Hostert, P., Dyk, A., et al., 2014. Pixel-based image compositing for large-area dense time series applications and science. Can. J. Remote. Sens. 40, 192–212.
White, J.C., Wulder, M.A., Hermosilla, T., Coops, N.C., Hobart, G.W., 2017. A nationwide annual characterization of 25 years of forest disturbance and recovery for Canada using Landsat time series. Remote Sens. Environ. 194, 303–321. http://dx.doi.org/10.1016/j.rse.2017.03.035.
Woodcock, C.E., Collins, J.B., Gopal, S., Jakabhazy, V.D., Li, X., Macomber, S., Ryherd, S., Harward, V.J., Levitan, J., Wu, Y., Warbington, R., 1994. Mapping forest vegetation using Landsat TM imagery and a canopy reflectance model. Remote Sens. Environ. 50, 240–254.
Woodcock, C.E., Allen, R., Anderson, M., Belward, A., Bindschadler, R., Cohen, W., Gao, F., Goward, S.N., Helder, D., Helmer, E., Nemani, R., 2008. Free access to Landsat imagery. Science 80 (320), 1011. http://dx.doi.org/10.1126/science.320.5879.1011a.
Wulder, M.A., Kurz, W.A., Gillis, M., 2004. National level forest monitoring and modeling in Canada. Prog. Plan. 61, 365–381.
Wulder, M.A., Bater, C.W., Coops, N.C., Hilker, T., White, J.C., 2008a. The role of LiDAR in sustainable forest management. For. Chron. 84, 807–826.
Wulder, M.A., White, J.C., Cranny, M., Hall, R.J., Luther, J.E., Beaudoin, A., Goodenough, D.G., Dechka, J.A., 2008b. Monitoring Canada's forests. Part 1: completion of the EOSD land cover project. Can. J. Remote. Sens. 34, 549–562.
Wulder, M.A., White, J.C., Bater, C.W., Coops, N.C., Hopkinson, C., Chen, G., 2012a. Lidar plots - a new large-area data collection option: context, concepts, and case study. Can. J. Remote. Sens. 38, 600–618. http://dx.doi.org/10.5589/m12-049.
Wulder, M.A., White, J.C., Nelson, R.F., Næsset, E., Ørka, H.O., Coops, N.C., Hilker, T., Bater, C.W., Gobakken, T., 2012b. Lidar sampling for large-area forest characterization: a review. Remote Sens. Environ. 121, 196–209. http://dx.doi.org/10.1016/j.rse.2012.02.001.
Wulder, M.A., White, J.C., Loveland, T.R., Woodcock, C.E., Belward, A.S., Cohen, W.B., Fosnight, E.A., Shaw, J., Masek, J.G., Roy, D.P., 2016. The global Landsat archive: status, consolidation, and direction. Remote Sens. Environ. 185, 271–283. http://dx.doi.org/10.1016/j.rse.2015.11.032.
Zald, H.S.J., Ohmann, J.L., Roberts, H.M., Gregory, M.J., Henderson, E.B., McGaughey, R.J., Braaten, J., 2014. Influence of lidar, Landsat imagery, disturbance history, plot location accuracy, and plot size on accuracy of imputation maps of forest composition and structure. Remote Sens. Environ. 143, 26–38.
Zald, H.S.J., Wulder, M.A., White, J.C., Hilker, T., Hermosilla, T., Hobart, G.W., Coops, N.C., 2016. Integrating Landsat pixel composites and change metrics with lidar plots to predictively map forest structure and aboveground biomass in Saskatchewan, Canada. Remote Sens. Environ. 176, 188–201. http://dx.doi.org/10.1016/j.rse.2016.01.015.
Zhu, Z., Woodcock, C.E., 2012. Object-based cloud and cloud shadow detection in Landsat imagery. Remote Sens. Environ. 118, 83–94.